International Journal of Solids and Structures 45 (2008) 5237–5257

Contents lists available at ScienceDirect

International Journal of Solids and Structures

journal homepage: www.elsevier.com/locate/ijsolstr

Interaction integrals for fracture analysis of functionally graded piezoelectric materials

B.N. Rao [a,*], M. Kuna [b]

[a] Structural Engineering Division, Department of Civil Engineering, Indian Institute of Technology, Madras, Chennai 600036, India
[b] TU Bergakademie Freiberg, Institut für Mechanik und Fluiddynamik, Lampadiusstraße 4, 09596 Freiberg, Germany

ARTICLE INFO

Article history:
Received 14 February 2008
Received in revised form 19 May 2008
Available online 3 June 2008

Keywords:
Crack
Functionally graded piezoelectric materials
Interaction integral
Non-equilibrium formulation
Incompatibility formulation
Constant constitutive tensor formulation
Displacement extrapolation method
Stress intensity factor
Electric displacement intensity factor

ABSTRACT

This paper presents domain form of the interaction integrals based on three independent formulations for computation of the stress intensity factors and electric displacement intensity factor for cracks in functionally graded piezoelectric materials. Conservation integrals of *J*-type are derived based on the governing equations for piezoelectric media and the crack tip asymptotic fields of homogeneous piezoelectric medium as auxiliary fields. Each of the formulation differs in the way auxiliary fields are imposed in the evaluation of interaction integral and each of them results in a consistent form of the interaction integral in the sense that extra terms naturally appears in their derivation to compensate for the difference in the chosen crack tip asymptotic fields of homogeneous and functionally graded piezoelectric medium. The additional terms play an important role of ensuring domain independence of the presented interaction integrals. Comparison of the numerically evaluated intensity factors through the three consistent formulations with those obtained using displacement extrapolation method is presented by means of two examples.

1. Introduction

Piezoelectric materials are widely used in many fields such as aerospace, automotive, medical and electronic technologies. While designing piezoelectric structures/components, it is important to take into account imperfections, such as cracks, that are often pre-existing or are generated by external loads during the service life. In recent years, emergence of the functionally graded materials (FGMs) has demonstrated that they have the potential to reduce the stress concentration and to increase the fracture toughness. Consequently, a new kind of material, such as a functionally graded piezoelectric material (FGPM), has been developed to improve the reliability of piezoelectric materials and structures by extending the concept of the well-known functionally graded material (FGM) to a piezoelectric material (Wu et al., 1996). For example, a device wholly made up of the FGPMs or using the FGPMs as a transit layer instead of the bonding agent avoids existence of discernible internal seams or boundaries. In addition, no internal stress peaks are caused when the voltage is applied and the failure due to development of internal de-bonding or stress peaks in conventional bimorphs can be avoided (Wu et al., 1996; Zhu et al., 2000). However, the microstructure of FGPM is generally heterogeneous, and the dominant type of failure in the FGPM is crack initiation and growth from inclusions. The extent to which constituent material properties and microstructure can be tailored to guard against potential fracture and failure patterns is relatively unknown. Such issues have motivated much of the current research into the numerical computation of crack driving forces in the FGPM, and several analytical studies concerned with the static fracture problems of the FGPMs were reported (Wang and Noda, 2001; Li and Weng, 2002; Wang and Zhang, 2004; Ma et al., 2005; Ueda, 2006, 2007, 2008). Thus, most of the studies on the FGPMs till today are analytical in

* Corresponding author. Tel.: +91 44 2257 4285; fax: +91 44 2257 5286.
E-mail address: bnrao@iitm.ac.in (B.N. Rao).

0020-7683/$ - see front matter © 2008 Elsevier Ltd. All rights reserved.
doi:10.1016/j.ijsolstr.2008.05.020

nature. As a result, there is considerable interest in developing numerical methods for the evaluation of crack driving force in the FGPMs. Recently, Sladek et al. (2007) developed a contour integral for computation of the stress intensity factors (SIFs) and electric displacement intensity factor (EDIF) for cracks in continuously non-homogeneous piezoelectric body subjected to transient dynamic load. To extract the mixed mode SIFs in FGMs the interaction integrals based on constant constitutive tensor formulations (Rao and Rahman, 2003a; Rao and Rahman, 2003b), incompatibility (Dolbow and Gosz, 2002; Rao and Rahman, 2003a; Rao and Rahman, 2003b) and non-equilibrium (Kim and Paulino, 2003; Paulino and Kim, 2004) have been developed.

In this paper domain form of the interaction integrals based on three independent formulations are presented for computation of the SIFs and EDIF for cracks in the FGPMs. To determine fracture parameters, e.g., the SIFs and EDIF, by means of the interaction integral method, the near crack tip electromechanical fields which are selected as auxiliary fields are needed. In fracture of the FGPMs, the use of the auxiliary fields developed for homogeneous piezoelectric materials results in violation of one of the three basic relations namely, equilibrium, compatibility, and constitutive, which leads to three independent formulations: non-equilibrium, incompatibility, and constant constitutive tensor formulations. Each formulation leads to a different final form of the resulting interaction integral, and for consistency, extra terms naturally appears in their derivation to compensate for the difference in the chosen crack tip asymptotic fields of homogeneous and functionally graded piezoelectric medium.

This paper is organized as follows. Section 2 briefly reviews basic equations for piezoelectric media. Section 3 presents crack tip fields in the FGPMs. Section 4 provides three consistent formulations using the interaction integral approach, proof of existence of the proposed integrals and the evaluation of intensity factors. Section 5 briefly describes displacement extrapolation method and illustrates the three formulations through two numerical examples. Finally, Section 6 concludes this work.

2. Basic equations for piezoelectric media

The elements of elasticity and electrostatics are combined in piezoelectric media. The governing equations and the boundary conditions which form the foundation of piezoelectric media are given below.

2.1. Field equations

In a fixed rectangular coordinate system x_j (j = 1–3), the field equations for a linear piezoelectric medium subjected to electromechanical loads in the absence of body forces and charges are

- Constitutive equations:

$$\sigma_{ij} = C_{ijks}\varepsilon_{ks} - e_{sij}E_s, \tag{1}$$

$$D_i = e_{iks}\varepsilon_{ks} + \kappa_{is}E_s, \tag{2}$$

- Kinematic equations:

$$\varepsilon_{ij} = \frac{1}{2}(u_{i,j} + u_{j,i}), E_i = -\phi_{,i}, \tag{3}$$

- Equilibrium equations:

$$\sigma_{ij,j} = 0, D_{i,i} = 0. \tag{4}$$

In Eqs. (3) and (4), a comma denotes partial differentiation, and the repeated indices summation; u_i is the component of the elastic displacement vector $\boldsymbol{u}$; ϕ is the electric potential; σ_{ij}, ε_{ij}, D_i, and E_i are the components of the stress, strain, electric displacement, and electric field, respectively; C_{ijks}, and e_{iks} are the elastic and piezoelectric constants, respectively; κ_{is} are the dielectric permitivities. Using the relation between the indices $11 \to 1$, $22 \to 2$, $33 \to 3$, $23 \to 4$, $31 \to 5$ and $12 \to 6$, the constitutive Eqs. (1) and (2) may be written in Voigt notation as: $\sigma_\alpha = C_{\alpha\beta}\varepsilon_\beta - e_{s\alpha}E_s$ and $D_i = e_{i\beta}\varepsilon_\beta + \kappa_{is}E_s$ respectively, where α, β = 1, …, 6, and i, s = 1–3.

2.2. Boundary conditions

Consider a piezoelectric medium occupying the space Ω. The surface of Ω is denoted as S and

$$S = S_\sigma + S_u = S_D + S_\phi. \tag{5}$$

On the boundaries S_σ, and S_D, the resultants of stresses and electric displacements are respectively:

$$\sigma_{ij}n_j = p_j^0, \quad \text{on } S_\sigma, \tag{6}$$

$$D_j n_j = \omega^0, \quad \text{on } S_D, \tag{7}$$

where p_j^0, and ω^0 are some prescribed values on S_σ, and S_D, respectively. $\boldsymbol{n}$ is the unit normal vector of S ($\boldsymbol{n}$ directed towards outside). On the boundaries S_u, and S_ϕ the displacement vector $\boldsymbol{u}$, and the electric potential ϕ, are respectively:

$$u_j = u_j^0, \quad \text{on } S_u, \tag{8}$$

$$\phi = \phi^0, \quad \text{on } S_\phi, \tag{9}$$

where u_j^0, and ϕ^0 are some prescribed values on S_u and S_ϕ, respectively.

3. Crack tip fields in functionally graded piezoelectric media

Consider a two-dimensional functionally graded piezoelectric structure with a rectilinear impermeable crack of length $2a$, subjected to external loads $p_1^0, p_2^0, \ldots, p_M^0$, and electrical displacement ω^0 as shown in Fig. 1. It is assumed that the material properties, such as C_{11}, C_{22}, C_{12}, C_{13}, C_{44}, e_{21}, e_{22}, e_{16}, κ_{11}, and κ_{22} (in Voigt notation), vary according to

$$(C_{11}, C_{22}, C_{12}, C_{13}, C_{44}, e_{21}, e_{22}, e_{16}, \kappa_{11}, \kappa_{22})(\boldsymbol{x}) = (C_{110}, C_{220}, C_{120}, C_{130}, C_{440}, e_{210}, e_{220}, e_{160}, \kappa_{110}, \kappa_{220}) f(x_1, x_2), \tag{10}$$

where $\boldsymbol{x} = \{x_1, x_2\}^{\mathrm{T}} \in \Re^2$, ($C_{11}$, C_{22},C_{12}, C_{13}, C_{44}, e_{21}, e_{22}, e_{16}, κ_{11},κ_{22}) ($\boldsymbol{x}$) are continuous, and at least piecewise differentiable functions on domain Ω, and the (x_1, x_2)-coordinate system is defined in Fig. 1. In reality, FGMPs are multiphase materials generally with locally discontinuous material properties. Hence, (C_{11}, C_{22}, C_{12}, C_{13}, C_{44}, e_{21}, e_{22}, e_{16}, κ_{11}, κ_{22}) ($\boldsymbol{x}$) in Eq. (10) should be viewed as smoothly varying "effective" material properties of FGMPs.

Eischen (1987) and Jin and Noda (1994) showed that for piecewise differentiable material property variations, the elastic stress and displacement fields in FGM can be derived using the stress function in variable separable form, identical to the homogeneous case. Similarly Sladek et al. (2007) showed that in case of the FGPMs the leading singularity is same as that for a homogenous piezoelectric body with material constants given by the crack tip values of the corresponding material parameters in the considered non-homogenous piezoelectric medium. For cracks in homogenous piezoelectric media the asymptotic behavior of the field quantities has been given by Sosa (1991) and Pak (1992). If polar coordinates (r, θ) with the origin at the crack tip are used, the electromechanical stress and electrical displacement fields can be written as

$$\sigma_{ij}(r,\theta) = \frac{1}{\sqrt{2\pi r}} \sum_N K_N f_{ij}^N(\theta), \tag{11}$$

$$D_i(r,\theta) = \frac{1}{\sqrt{2\pi r}} \sum_N K_N g_i^N(\theta), \tag{12}$$

and, the near tip displacement field and electric potential can be obtained as

$$u_i(r,\theta) = \sqrt{\frac{2r}{\pi}} \sum_N K_N d_i^N(\theta), \tag{13}$$

$$\phi(r,\theta) = \sqrt{\frac{2r}{\pi}} \sum_N K_N v^N(\theta), \tag{14}$$

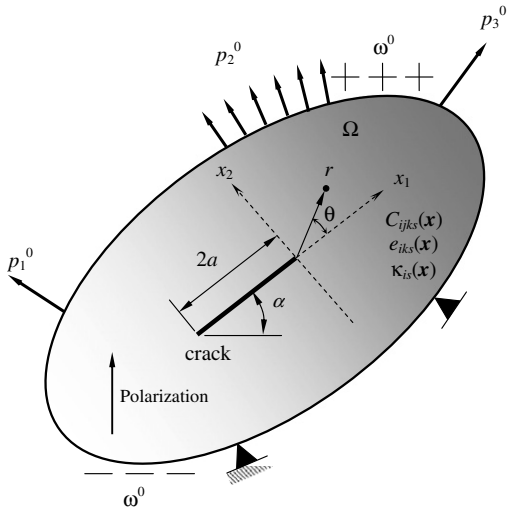

Fig. 1. A crack in functionally graded piezoelectric material.

where $i, j = 1–2$, and the summation over $N = \{\text{II, I, III, IV}\}$ comprises the fracture opening modes, usually indicated by roman letters. K_{I}, K_{II} and K_{III} denote the well known mode-I, mode-II, mode-III, mechanical SIFs and K_{IV} denote the EDIF characterizing the concentration of the electrical displacement fields. For two-dimensional functionally graded piezoelectric structure as shown in Fig. 1, $K_{\text{III}} = 0$. The angular functions $f_{ij}^N(\theta)$, $g_i^N(\theta)$, $d_i^N(\theta)$, and $v^N(\theta)$, are the standard angular functions for a crack in a homogeneous piezoelectric elastic medium, which depend only on the material properties, and can be found by means of the extended Stroh formalism and semi-analytical calculations. They can be expressed in terms of complex material eigenvalues p_α, eigenvectors $A_{M\alpha}$, and matrices $M_{M\alpha}$ and $N_{\alpha N}$ (Park and Sun, 1995; Ricoeur and Kuna, 2003; Kuna, 2006) as

$$f_{i1}^N = -\sum_{\alpha=1}^{4} \mathrm{Re}\left\{\frac{M_{i\alpha}N_{\alpha N}p_\alpha}{\sqrt{\cos\theta + p_\alpha \sin\theta}}\right\}, \quad f_{i2}^N = \sum_{\alpha=1}^{4} \mathrm{Re}\left\{\frac{M_{i\alpha}N_{\alpha N}}{\sqrt{\cos\theta + p_\alpha \sin\theta}}\right\},$$
$$g_1^N = -\sum_{\alpha=1}^{4} \mathrm{Re}\left\{\frac{M_{4\alpha}N_{\alpha N}p_\alpha}{\sqrt{\cos\theta + p_\alpha \sin\theta}}\right\}, \quad g_2^N = \sum_{\alpha=1}^{4} \mathrm{Re}\left\{\frac{M_{4\alpha}N_{\alpha N}}{\sqrt{\cos\theta + p_\alpha \sin\theta}}\right\}, \tag{15}$$

$$d_i^N = \sum_{\alpha=1}^{4} \mathrm{Re}\left\{A_{i\alpha}N_{\alpha N}\sqrt{\cos\theta + p_\alpha \sin\theta}\right\}, \quad v^N = \sum_{\alpha=1}^{4} \mathrm{Re}\left\{A_{4\alpha}N_{\alpha N}\sqrt{\cos\theta + p_\alpha \sin\theta}\right\}, \tag{16}$$

where $\mathrm{Re}\{\ldots\}$ and $\mathrm{Im}\{\ldots\}$ denote the real part and the imaginary part respectively of the quantity in brackets. The four conjugate pairs of eigenvalues p_α, the (4×4) matrix of eigenvectors $A_{M\alpha}$ which depends only on material properties, not on the boundary value problem itself can be obtained by solving the following quadratic, eigenvalue problem:

$$\left[\begin{pmatrix} C_{i1k1} & e_{i11} \\ e_{1k1} & -\kappa_{11} \end{pmatrix} + \begin{pmatrix} C_{i2k1} + C_{i1k2} & e_{i21} + e_{i12} \\ e_{2k1} + e_{1k2} & -\kappa_{12} - \kappa_{21} \end{pmatrix} p + \begin{pmatrix} C_{i2k2} & e_{i22} \\ e_{2k2} & -\kappa_{22} \end{pmatrix} p^2 \right] \begin{bmatrix} A_i \\ A_4 \end{bmatrix} = \boldsymbol{0}. \tag{17}$$

Only the four eigenvalues p_α, having positive imaginary part and the corresponding eigenvectors are used in Eqs. (15) and (16). The (4×4) matrices $M_{M\alpha}$ and $N_{\alpha N}$ are calculated by

$$N_{\alpha N}^{-1} = M_{M\alpha} = \begin{bmatrix} (C_{i2k1} + C_{i2k2}p_\alpha)A_{k\alpha} & (e_{1i2} + e_{2i2}p_\alpha)A_{4\alpha} \\ (e_{2k1} + e_{2k2}p_\alpha)A_{k\alpha} & (-\kappa_{21} - \kappa_{22}p_\alpha)A_{4\alpha} \end{bmatrix}. \tag{18}$$

Even though the material gradient does not influence the square-root singularity or the singular stress and electrical displacement distribution, the material gradient does affect the SIFs and EDIF. Hence, the fracture parameters are functions of the material gradients, external loading, and geometry.

4. Interaction integral formulations

The interaction integral method is an effective tool for calculating the SIFs and EDIF in homogeneous piezoelectric materials (Enderlein et al., 2005; Kuna, 2006). In this section the interaction integral method for homogeneous piezoelectric materials is first briefly summarized, then extended for cracks in the FGPM. In fact, the study of the FGPM would enhance the understanding of a fracture in a generic piezoelectric material, since upon shrinking, the gradient layer in the FGPM is expected to behave like a sharp interface, and upon expansion, the fracture behavior would be analogous to that of a homogeneous piezoelectric material.

4.1. Homogeneous piezoelectric materials

The path independent electromechanical J-integral for a homogeneous piezoelectric cracked body is given by (Cherepanov, 1977; Pak and Herrmann, 1986; Pak, 1990)

$$J = \int_\Gamma \left(H\delta_{1j} - \sigma_{ij}\frac{\partial u_i}{\partial x_1} - D_j\frac{\partial \phi}{\partial x_1}\right) n_j \, \mathrm{d}\Gamma, \tag{19}$$

where $H = \int \sigma_{ij}\mathrm{d}\varepsilon_{ij} - \int D_i \mathrm{d}E_i$ is the electric enthalpy density, n_j is the jth component of the outward unit vector normal to an arbitrary contour Γ enclosing the crack tip and δ_{ij} is the Kronecker delta. For linear piezoelectric material models it can be shown that $H = (\sigma_{ij}\varepsilon_{ij} - D_i E_i)/2 = C_{ijkl}\varepsilon_{ij}\varepsilon_{kl}/2 - e_{ikl}\varepsilon_{kl}E_i - \kappa_{im}E_iE_m/2$. Applying the divergence theorem, the contour integral in Eq. (19) can be converted into an equivalent domain form, given by

$$J = \int_A \left(\sigma_{ij}\frac{\partial u_i}{\partial x_1} + D_j\frac{\partial \phi}{\partial x_1} - H\delta_{1j}\right)\frac{\partial q}{\partial x_j}\mathrm{d}A + \int_A \frac{\partial}{\partial x_j}\left(\sigma_{ij}\frac{\partial u_i}{\partial x_1} + D_j\frac{\partial \phi}{\partial x_1} - H\delta_{1j}\right) q \, \mathrm{d}A, \tag{20}$$

where A is the area inside the contour Γ and q is a smooth weight function chosen such that it has a value of *unity* at the crack tip, *zero* along the boundary of the domain Γ, and smoothly interpolated in between (Anderson, 2005). By expanding the second integrand, Eq. (20) reduces to

$$J=\int_A\left(\sigma_{ij}\frac{\partial u_i}{\partial x_1}+D_j\frac{\partial\phi}{\partial x_1}-H\delta_{1j}\right)\frac{\partial q}{\partial x_j}\,\mathrm{d}A+\int_A\begin{pmatrix}\frac{\partial\sigma_{ij}}{\partial x_j}\frac{\partial u_i}{\partial x_1}+\sigma_{ij}\frac{\partial^2 u_i}{\partial x_j\partial x_1}+\frac{\partial D_j}{\partial x_j}\frac{\partial\phi}{\partial x_1}+D_j\frac{\partial^2\phi}{\partial x_j\partial x_1}\\ -C_{ijkl}\varepsilon_{ij}\frac{\partial\varepsilon_{kl}}{\partial x_1}-\frac{1}{2}\varepsilon_{ij}\frac{\partial C_{ijkl}}{\partial x_1}\varepsilon_{kl}+\varepsilon_{kl}\frac{\partial e_{ikl}}{\partial x_1}E_i+\frac{\partial\varepsilon_{kl}}{\partial x_1}e_{ikl}E_i\\ +\varepsilon_{kl}e_{ikl}\frac{\partial E_i}{\partial x_1}+E_i\kappa_{im}\frac{\partial E_m}{\partial x_1}+\frac{1}{2}E_i\frac{\partial\kappa_{im}}{\partial x_1}E_m\end{pmatrix}q\;\mathrm{d}A. \tag{21}$$

Using equilibrium ($\partial\sigma_{ij}/\partial x_j=0,\partial D_i/\partial x_i=0$) and compatibility ($\varepsilon_{ij}=(\partial u_i/\partial x_j+\partial u_j/\partial x_i)/2, E_i=-\partial\phi/\partial x_i$) conditions and noting that $\partial C_{ijkl}/\partial x_1=0$, $\partial e_{ikl}/\partial x_1=0$, $\partial\kappa_{im}/\partial x_1=0$ in homogenous piezoelectric materials, the second integrand of Eq. (21) vanishes, yielding

$$J=\int_A\left(\sigma_{ij}\frac{\partial u_i}{\partial x_1}+D_j\frac{\partial\phi}{\partial x_1}-H\delta_{1j}\right)\frac{\partial q}{\partial x_j}\,\mathrm{d}A, \tag{22}$$

which is the domain form of the electromechanical J-integral in homogenous piezoelectric materials.

Next, we consider two independent equilibrium states of the cracked body. Let state 1 correspond to the *actual* state for the given boundary conditions, and let state 2 correspond to an *auxiliary* state, which can be near tip electromechanical fields of any of the fracture opening modes I, II, III, and IV. Superposition of these two states leads to another equilibrium state (state S) for which the domain form of the J-integral is

$$J^{(S)}=\int_A\left((\sigma_{ij}^{(1)}+\sigma_{ij}^{(2)})\frac{\partial(u_i^{(1)}+u_i^{(2)})}{\partial x_1}+(D_j^{(1)}+D_j^{(2)})\frac{\partial(\phi^{(1)}+\phi^{(2)})}{\partial x_1}-H^{(S)}\delta_{1j}\right)\frac{\partial q}{\partial x_j}\,\mathrm{d}A, \tag{23}$$

where superscript $i=1$, 2, and S indicate fields and quantities associated with state i and

$$H^{(S)}=((\sigma_{ij}^{(1)}+\sigma_{ij}^{(2)})(\varepsilon_{ij}^{(1)}+\varepsilon_{ij}^{(2)})-(D_j^{(1)}+D_j^{(2)})(E_j^{(1)}+E_j^{(2)}))/2. \tag{24}$$

By expanding Eq. (23)

$$J^{(S)}=J^{(1)}+J^{(2)}+M^{(1,2)}, \tag{25}$$

where

$$J^{(1)}=\int_A\left(\sigma_{ij}^{(1)}\frac{\partial u_i^{(1)}}{\partial x_1}+D_j^{(1)}\frac{\partial\phi^{(1)}}{\partial x_1}-H^{(1)}\delta_{1j}\right)\frac{\partial q}{\partial x_j}\,\mathrm{d}A, \tag{26}$$

and

$$J^{(2)}=\int_A\left(\sigma_{ij}^{(2)}\frac{\partial u_i^{(2)}}{\partial x_1}+D_j^{(2)}\frac{\partial\phi^{(2)}}{\partial x_1}-H^{(2)}\delta_{1j}\right)\frac{\partial q}{\partial x_j}\,\mathrm{d}A, \tag{27}$$

are the electromechanical J-integrals for states 1 and 2, respectively, and

$$M^{(1,2)}=\int_A\left(\sigma_{ij}^{(1)}\frac{\partial u_i^{(2)}}{\partial x_1}+D_j^{(1)}\frac{\partial\phi^{(2)}}{\partial x_1}+\sigma_{ij}^{(2)}\frac{\partial u_i^{(1)}}{\partial x_1}+D_j^{(2)}\frac{\partial\phi^{(1)}}{\partial x_1}-H^{(1,2)}\delta_{1j}\right)\frac{\partial q}{\partial x_j}\,\mathrm{d}A, \tag{28}$$

is an interaction integral. In Eqs. (26)–(28), $H^{(1)}=(\sigma_{ij}^{(1)}\varepsilon_{ij}^{(1)}-D_j^{(1)}E_j^{(1)})/2$, $H^{(2)}=(\sigma_{ij}^{(2)}\varepsilon_{ij}^{(2)}-D_j^{(2)}E_j^{(2)})/2$, and $H^{(1,2)}=(\sigma_{ij}^{(1)}\varepsilon_{ij}^{(2)}+\sigma_{ij}^{(2)}\varepsilon_{ij}^{(1)}-D_j^{(1)}E_j^{(2)}-D_j^{(2)}E_j^{(1)})/2$ represent various electric enthalpy densities, which satisfy

$$H^{(S)}=H^{(1)}+H^{(2)}+H^{(1,2)}. \tag{29}$$

For linear piezoelectric solids under mixed-mode loading conditions, the electromechanical J-integral is also equal to the energy release rate and hence, the electromechanical J-integral can be written as (Kuna, 2006)

$$J=\frac{1}{2}\boldsymbol{K}^{\mathrm{T}}\boldsymbol{Y}\boldsymbol{K}, \tag{30}$$

where $\boldsymbol{K}=\{K_{\mathrm{II}}\quad K_{\mathrm{I}}\quad K_{\mathrm{III}}\quad K_{\mathrm{IV}}\}^{\mathrm{T}}$ is the vector of the four field intensity factors, and $\boldsymbol{Y}$ is the (4×4) generalized Irwin matrix, which depends on the elastic, piezoelectric, and dielectric material constants is given by

$$Y_{\mathrm{MN}}=-\mathrm{Im}\{A_{M\alpha}N_{\alpha N}\}. \tag{31}$$

For two-dimensional case, Equation (30) reduces to,

$$J=\frac{1}{2}K_{\mathrm{II}}^2Y_{11}+\frac{1}{2}K_{\mathrm{I}}^2Y_{22}+\frac{1}{2}K_{\mathrm{IV}}^2Y_{44}+K_{\mathrm{I}}K_{\mathrm{II}}Y_{12}+K_{\mathrm{II}}K_{\mathrm{IV}}Y_{14}+K_{\mathrm{I}}K_{\mathrm{IV}}Y_{24}. \tag{32}$$

Applying Eq. (32) to states 1, 2, and the superimposed state S gives

$$J^{(1)}=\frac{1}{2}K_{\mathrm{II}}^{(1)2}Y_{11}+\frac{1}{2}K_{\mathrm{I}}^{(1)2}Y_{22}+\frac{1}{2}K_{\mathrm{IV}}^{(1)2}Y_{44}+K_{\mathrm{I}}^{(1)}K_{\mathrm{II}}^{(1)}Y_{12}+K_{\mathrm{II}}^{(1)}K_{\mathrm{IV}}^{(1)}Y_{14}+K_{\mathrm{I}}^{(1)}K_{\mathrm{IV}}^{(1)}Y_{24}, \tag{33}$$

$$J^{(2)}=\frac{1}{2}K_{\mathrm{II}}^{(2)2}Y_{11}+\frac{1}{2}K_{\mathrm{I}}^{(2)2}Y_{22}+\frac{1}{2}K_{\mathrm{IV}}^{(2)2}Y_{44}+K_{\mathrm{I}}^{(2)}K_{\mathrm{II}}^{(2)}Y_{12}+K_{\mathrm{II}}^{(2)}K_{\mathrm{IV}}^{(2)}Y_{14}+K_{\mathrm{I}}^{(2)}K_{\mathrm{IV}}^{(2)}Y_{24}, \tag{34}$$

and

$$J^{(S)} = J^{(1)} + J^{(2)} + K_{\mathrm{II}}^{(1)}K_{\mathrm{II}}^{(2)}Y_{11} + K_{\mathrm{I}}^{(1)}K_{\mathrm{I}}^{(2)}Y_{22} + K_{\mathrm{IV}}^{(1)}K_{\mathrm{IV}}^{(2)}Y_{44} + (K_{\mathrm{I}}^{(1)}K_{\mathrm{II}}^{(2)} + K_{\mathrm{II}}^{(1)}K_{\mathrm{I}}^{(2)})Y_{12} + (K_{\mathrm{II}}^{(1)}K_{\mathrm{IV}}^{(2)} + K_{\mathrm{IV}}^{(1)}K_{\mathrm{II}}^{(2)})Y_{14} + (K_{\mathrm{I}}^{(1)}K_{\mathrm{IV}}^{(2)} + K_{\mathrm{IV}}^{(1)}K_{\mathrm{I}}^{(2)})Y_{24}. \tag{35}$$

Comparing Eqs. (25) and (35)

$$M^{(1,2)} = K_{\mathrm{II}}^{(1)}K_{\mathrm{II}}^{(2)}Y_{11} + K_{\mathrm{I}}^{(1)}K_{\mathrm{I}}^{(2)}Y_{22} + K_{\mathrm{IV}}^{(1)}K_{\mathrm{IV}}^{(2)}Y_{44} + (K_{\mathrm{I}}^{(1)}K_{\mathrm{II}}^{(2)} + K_{\mathrm{II}}^{(1)}K_{\mathrm{I}}^{(2)})Y_{12} + (K_{\mathrm{II}}^{(1)}K_{\mathrm{IV}}^{(2)} + K_{\mathrm{IV}}^{(1)}K_{\mathrm{II}}^{(2)})Y_{14} + (K_{\mathrm{I}}^{(1)}K_{\mathrm{IV}}^{(2)} + K_{\mathrm{IV}}^{(1)}K_{\mathrm{I}}^{(2)})Y_{24}. \tag{36}$$

The individual SIFs and EDIF for the actual state can be obtained by judiciously choosing the auxiliary state (state 2). For example, if state 2 is chosen to be near tip displacement and stress field corresponding to the fracture opening mode I, then $K_{\mathrm{I}}^{(2)} = 1$, $K_{\mathrm{II}}^{(2)} = 0$, and $K_{\mathrm{IV}}^{(2)} = 0$. Hence, Eq. (36) can be reduced to

$$M^{(1,\mathrm{I})} = K_{\mathrm{I}}^{(1)}Y_{22} + K_{\mathrm{II}}^{(1)}Y_{12} + K_{\mathrm{IV}}^{(1)}Y_{24}. \tag{37}$$

Similarly, if state 2 is chosen to be near tip displacement and stress field corresponding to the fracture opening mode II, with $K_{\mathrm{I}}^{(2)} = 0$, $K_{\mathrm{II}}^{(2)} = 1$, and $K_{\mathrm{IV}}^{(2)} = 0$ and if state 2 is chosen to be near tip displacement and stress field corresponding to the fracture opening mode IV, with $K_{\mathrm{I}}^{(2)} = 0$, $K_{\mathrm{II}}^{(2)} = 0$, and $K_{\mathrm{IV}}^{(2)} = 1$, then Eq. (36) reduces to

$$M^{(1,\mathrm{II})} = K_{\mathrm{I}}^{(1)}Y_{12} + K_{\mathrm{II}}^{(1)}Y_{11} + K_{\mathrm{IV}}^{(1)}Y_{14}, \tag{38}$$

and

$$M^{(1,\mathrm{IV})} = K_{\mathrm{I}}^{(1)}Y_{24} + K_{\mathrm{II}}^{(1)}Y_{14} + K_{\mathrm{IV}}^{(1)}Y_{44}, \tag{39}$$

respectively.

Solving the simultaneous Eqs. (37)–(39), $K_{\mathrm{I}}^{(1)}$, $K_{\mathrm{II}}^{(1)}$, and $K_{\mathrm{IV}}^{(1)}$ can be obtained. The interaction integrals $M^{(1,\mathrm{I})}$, $M^{(1,\mathrm{II})}$ and $M^{(1,\mathrm{IV})}$ can be evaluated from Eq. (28). Eqs. (37)–(39) have been successfully used for calculating the SIFs and EDIF in homogenous piezoelectric materials under various mixed-mode loading conditions (Enderlein et al., 2005; Kuna, 2006).

4.2. Functionally graded piezoelectric materials

For non-homogeneous piezoelectric materials, even though the equilibrium and compatibility conditions are satisfied, the material gradient term of the second integrand of Eq. (21) does not vanish. So Eq. (21) reduces to a more general integral, henceforth referred to as the electromechanical $\widetilde{J}$-integral, which is

$$\widetilde{J} = \int_A \left(\sigma_{ij}\frac{\partial u_i}{\partial x_1} + D_j\frac{\partial \phi}{\partial x_1} - H\delta_{1j}\right)\frac{\partial q}{\partial x_j}\,\mathrm{d}A - \int_A \left(\frac{1}{2}\varepsilon_{ij}\frac{\partial C_{ijkl}}{\partial x_1}\varepsilon_{kl} - \varepsilon_{kl}\frac{\partial e_{ikl}}{\partial x_1}E_i - \frac{1}{2}E_i\frac{\partial \kappa_{im}}{\partial x_1}E_m\right)q\ \mathrm{d}A. \tag{40}$$

By comparing Eq. (40) to the electromechanical J-integral (see Eq. (22)), the presence of material non-homogeneity results in the addition of the second domain integral. Although this integral is negligible for a path very close to the crack tip, it must be accounted for with relatively large integral domains, so that the electromechanical $\widetilde{J}$-integral can be accurately calculated.

The electromechanical $\widetilde{J}$-integral also represents the energy release rate of piezoelectric body. It is elementary to show that the electromechanical $\widetilde{J}$-integral becomes *zero* for any closed contour in an uncracked homogeneous piezoelectric, as well as in non-homogeneous piezoelectric bodies, and therefore remains path independent when used in conjunction with cracks in the FGPMs.

In order to derive the interaction integral for the FGPMs, consider again actual (state 1), auxiliary (state 2), and superimposed (state S) equilibrium states. For the actual state, Eq. (40) can be directly invoked to represent the electromechanical $\widetilde{J}$-integral. However, a more general form, such as Eq. (20), must be used for auxiliary and superimposed states. For example, the electromechanical $\widetilde{J}$-integral for the superimposed state S can be written as

$$\widetilde{J}^{(S)} = \int_A \left((\sigma_{ij}^{(1)} + \sigma_{ij}^{(2)})\frac{\partial(u_i^{(1)} + u_i^{(2)})}{\partial x_1} + (D_j^{(1)} + D_j^{(2)})\frac{\partial(\phi^{(1)} + \phi^{(2)})}{\partial x_1} - H^{(S)}\delta_{1j}\right)\frac{\partial q}{\partial x_j}\,\mathrm{d}A + \int_A \frac{\partial}{\partial x_j}\left((\sigma_{ij}^{(1)} + \sigma_{ij}^{(2)})\frac{\partial(u_i^{(1)} + u_i^{(2)})}{\partial x_1} + (D_j^{(1)} + D_j^{(2)})\frac{\partial(\phi^{(1)} + \phi^{(2)})}{\partial x_1} - H^{(S)}\delta_{1j}\right)q\ \mathrm{d}A. \tag{41}$$

Clearly, the evaluations of $\widetilde{J}^{(S)}$ and the resulting interaction integral depends on how the auxiliary field is defined. There are several options in choosing the auxiliary field. Three methods, studied in this paper, are described in the following.

4.2.1. Method I – constant constitutive tensor formulation

The method I involves selecting the auxiliary stress, electrical displacement, displacement fields and electric potential given by Eqs. (11)–(14) and calculating the auxiliary strain and electric fields from the symmetric gradient of the auxiliary displacement field and the gradient of the auxiliary electric potential. In this approach, the auxiliary stress, and electrical

displacement are related to the auxiliary strain, and electrical fields through a constant constitutive tensor comprising of the elastic, piezoelectric and dielectric material constants, evaluated at the crack tip. Hence, both equilibrium ($\partial\sigma_{ij}^{(2)}/\partial x_j = 0, \partial D_i^{(2)}/\partial x_i = 0$) and compatibility ($\varepsilon_{ij}^{(2)} = (\partial u_i^{(2)}/\partial x_j + \partial u_j^{(2)}/\partial x_i)/2, E_i^{(2)} = -\partial\phi^{(2)}/\partial x_i$) conditions are satisfied in the auxiliary state. However, the non-homogeneous constitutive relation of the FGPM is not strictly satisfied in the auxiliary state, which would introduce gradients of stress fields as extra terms in the interaction integral.

Using Eq. (29) and invoking both equilibrium and compatibility conditions, Eq. (41) can be further simplified to

$$\widetilde{J}^{(S)} = \int_A \begin{pmatrix} (\sigma_{ij}^{(1)} + \sigma_{ij}^{(2)})\frac{\partial(u_i^{(1)}+u_i^{(2)})}{\partial x_1} + (D_j^{(1)} + D_j^{(2)})\frac{\partial(\phi^{(1)}+\phi^{(2)})}{\partial x_1} \\ -(H^{(1)} + H^{(2)} + H^{(1,2)})\delta_{1j} \end{pmatrix} \frac{\partial q}{\partial x_j} \mathrm{d}A + \int_A \begin{pmatrix} -\frac{1}{2}\varepsilon_{ij}^{(1)}\frac{\partial C_{ijkl}}{\partial x_1}\varepsilon_{kl}^{(1)} + \varepsilon_{kl}^{(1)}\frac{\partial e_{jkl}}{\partial x_1}E_j^{(1)} + \frac{1}{2}E_k^{(1)}\frac{\partial \kappa_{jk}}{\partial x_1}E_j^{(1)} \\ +\frac{1}{2}\sigma_{ij}^{(1)}\frac{\partial \varepsilon_{ij}^{(2)}}{\partial x_1} - \frac{1}{2}\frac{\partial \sigma_{ij}^{(1)}}{\partial x_1}\varepsilon_{ij}^{(2)} + \frac{1}{2}\sigma_{ij}^{(2)}\frac{\partial \varepsilon_{ij}^{(1)}}{\partial x_1} - \frac{1}{2}\frac{\partial \sigma_{ij}^{(2)}}{\partial x_1}\varepsilon_{ij}^{(1)} \\ -\frac{1}{2}D_j^{(1)}\frac{\partial E_j^{(2)}}{\partial x_1} + \frac{1}{2}\frac{\partial D_j^{(1)}}{\partial x_1}E_j^{(2)} - \frac{1}{2}D_j^{(2)}\frac{\partial E_j^{(1)}}{\partial x_1} + \frac{1}{2}\frac{\partial D_j^{(2)}}{\partial x_1}E_j^{(1)} \end{pmatrix} q \, \mathrm{d}A. \tag{42}$$

By expanding Eq. (42),

$$\widetilde{J}^{(S)} = \widetilde{J}^{(1)} + \widetilde{J}^{(2)} + \widetilde{M}^{(1,2)}, \tag{43}$$

where

$$\widetilde{J}^{(1)} = \int_A \left(\sigma_{ij}^{(1)}\frac{\partial u_i^{(1)}}{\partial x_1} + D_j^{(1)}\frac{\partial \phi^{(1)}}{\partial x_1} - H^{(1)}\delta_{1j}\right)\frac{\partial q}{\partial x_j}\mathrm{d}A - \int_A \left(\frac{1}{2}\varepsilon_{ij}^{(1)}\frac{\partial C_{ijkl}}{\partial x_1}\varepsilon_{kl}^{(1)} - \varepsilon_{kl}^{(1)}\frac{\partial e_{jkl}}{\partial x_1}E_j^{(1)} - \frac{1}{2}E_k^{(1)}\frac{\partial \kappa_{jk}}{\partial x_1}E_j^{(1)}\right) q \, \mathrm{d}A, \tag{44}$$

$$\widetilde{J}^{(2)} = \int_A \left(\sigma_{ij}^{(2)}\frac{\partial u_i^{(2)}}{\partial x_1} + D_j^{(2)}\frac{\partial \phi^{(2)}}{\partial x_1} - H^{(2)}\delta_{1j}\right)\frac{\partial q}{\partial x_j}\mathrm{d}A, \tag{45}$$

are the electromechanical $\widetilde{J}$-integrals for states 1 and 2, respectively, and

$$\widetilde{M}^{(1,2)} = \int_A \left(\sigma_{ij}^{(1)}\frac{\partial u_i^{(2)}}{\partial x_1} + \sigma_{ij}^{(2)}\frac{\partial u_i^{(1)}}{\partial x_1} + D_j^{(1)}\frac{\partial \phi^{(2)}}{\partial x_1} + D_j^{(2)}\frac{\partial \phi^{(1)}}{\partial x_1} - H^{(1,2)}\delta_{1j}\right)\frac{\partial q}{\partial x_j}\mathrm{d}A + \int_A \frac{1}{2}\begin{pmatrix} \sigma_{ij}^{(1)}\frac{\partial \varepsilon_{ij}^{(2)}}{\partial x_1} - \frac{\partial \sigma_{ij}^{(1)}}{\partial x_1}\varepsilon_{ij}^{(2)} + \sigma_{ij}^{(2)}\frac{\partial \varepsilon_{ij}^{(1)}}{\partial x_1} - \frac{\partial \sigma_{ij}^{(2)}}{\partial x_1}\varepsilon_{ij}^{(1)} \\ -D_j^{(1)}\frac{\partial E_j^{(2)}}{\partial x_1} + \frac{\partial D_j^{(1)}}{\partial x_1}E_j^{(2)} - D_j^{(2)}\frac{\partial E_j^{(1)}}{\partial x_1} + \frac{\partial D_j^{(2)}}{\partial x_1}E_j^{(1)} \end{pmatrix} q \, \mathrm{d}A, \tag{46}$$

is the modified interaction integral for non-homogeneous piezoelectric materials.

4.2.2. Method II – incompatibility formulation

The method II entails selecting the auxiliary stress, electrical displacement, displacement fields and electric potential given by Eqs. (11)–(14) and calculating the auxiliary strain and electric fields using the same spatially varying elastic, piezoelectric and dielectric material tensors of the FGPM. In this approach, the auxiliary stress and electrical displacement fields satisfies equilibrium ($\partial\sigma_{ij}^{(2)}/\partial x_j = 0, \partial D_i^{(2)}/\partial x_i = 0$); however, the auxiliary strain and electric fields are not compatible with the auxiliary displacement fields and electric potential ($\varepsilon_{ij}^{(2)} \neq (\partial u_i^{(2)}/\partial x_j + \partial u_j^{(2)}/\partial x_i)/2, E_i^{(2)} \neq -\partial\phi^{(2)}/\partial x_i$). If the auxiliary fields are not compatible, extra terms that will arise due to lack of compatibility should be taken into account while evaluating the interaction integral. Hence, this method also introduces additional terms to the resulting interaction integral.

Following similar considerations, but using only equilibrium condition in the auxiliary state, Eq. (41) can also be simplified to

$$\widetilde{J}^{(S)} = \int_A \begin{pmatrix} (\sigma_{ij}^{(1)} + \sigma_{ij}^{(2)})\frac{\partial(u_i^{(1)}+u_i^{(2)})}{\partial x_1} + (D_j^{(1)} + D_j^{(2)})\frac{\partial(\phi^{(1)}+\phi^{(2)})}{\partial x_1} \\ -(H^{(1)} + H^{(2)} + H^{(1,2)})\delta_{1j} \end{pmatrix} \frac{\partial q}{\partial x_j} \mathrm{d}A + \int_A \begin{pmatrix} (\sigma_{ij}^{(1)} + \sigma_{ij}^{(2)})\left(\frac{\partial^2 u_i^{(2)}}{\partial x_j \partial x_1} - \frac{\partial \varepsilon_{ij}^{(2)}}{\partial x_1}\right) + (D_j^{(1)} + D_j^{(2)})\left(\frac{\partial^2 \phi^{(2)}}{\partial x_j \partial x_1} + \frac{\partial E_j^{(2)}}{\partial x_1}\right) \\ -\frac{1}{2}(\varepsilon_{ij}^{(1)} + \varepsilon_{ij}^{(2)})\frac{\partial C_{ijkl}}{\partial x_1}(\varepsilon_{kl}^{(1)} + \varepsilon_{kl}^{(2)}) + (E_n^{(1)} + E_n^{(2)})\frac{\partial e_{nkl}}{\partial x_1}(\varepsilon_{kl}^{(1)} + \varepsilon_{kl}^{(2)}) \\ +\frac{1}{2}(E_n^{(1)} + E_n^{(2)})\frac{\partial \kappa_{nm}}{\partial x_1}(E_m^{(1)} + E_m^{(2)}) \end{pmatrix} q \, \mathrm{d}A \tag{47}$$

Comparing Eqs. (47) and (43)

$$\widetilde{J}^{(1)} = \int_A \left(\sigma_{ij}^{(1)}\frac{\partial u_i^{(1)}}{\partial x_1} + D_j^{(1)}\frac{\partial \phi^{(1)}}{\partial x_1} - H^{(1)}\delta_{1j}\right)\frac{\partial q}{\partial x_j}\mathrm{d}A - \int_A \left(\frac{1}{2}\varepsilon_{ij}^{(1)}\frac{\partial C_{ijkl}}{\partial x_1}\varepsilon_{kl}^{(1)} - \varepsilon_{kl}^{(1)}\frac{\partial e_{ikl}}{\partial x_1}E_i^{(1)} - \frac{1}{2}E_i^{(1)}\frac{\partial \kappa_{im}}{\partial x_1}E_m^{(1)}\right) q \, \mathrm{d}A, \tag{48}$$

$$\widetilde{J}^{(2)} = \int_A \left(\sigma_{ij}^{(2)}\frac{\partial u_i^{(2)}}{\partial x_1} + D_j^{(2)}\frac{\partial \phi^{(2)}}{\partial x_1} - H^{(2)}\delta_{1j}\right)\frac{\partial q}{\partial x_j}\mathrm{d}A + \int_A \begin{pmatrix} \sigma_{ij}^{(2)}\left(\frac{\partial^2 u_i^{(2)}}{\partial x_j \partial x_1} - \frac{\partial \varepsilon_{ij}^{(2)}}{\partial x_1}\right) + D_j^{(2)}\left(\frac{\partial^2 \phi^{(2)}}{\partial x_j \partial x_1} + \frac{\partial E_j^{(2)}}{\partial x_1}\right) \\ -\frac{1}{2}\varepsilon_{ij}^{(2)}\frac{\partial C_{ijkl}}{\partial x_1}\varepsilon_{kl}^{(2)} + E_n^{(2)}\frac{\partial e_{nkl}}{\partial x_1}\varepsilon_{kl}^{(2)} + \frac{1}{2}E_n^{(2)}\frac{\partial \kappa_{nm}}{\partial x_1}E_m^{(2)} \end{pmatrix} q \, \mathrm{d}A \tag{49}$$

are the electromechanical $\widetilde{J}$-integrals for states 1 and 2, respectively, and

$$\widetilde{M}^{(1,2)} = \int_A \left(\sigma_{ij}^{(1)} \frac{\partial u_i^{(1)}}{\partial x_1} + \sigma_{ij}^{(2)} \frac{\partial u_i^{(1)}}{\partial x_1} + D_j^{(1)} \frac{\partial \phi^{(2)}}{\partial x_1} + D_j^{(2)} \frac{\partial \phi^{(1)}}{\partial x_1} - H^{(1,2)} \delta_{1j} \right) \frac{\partial q}{\partial x_j} \mathrm{d}A + \int_A \left(\begin{array}{c} \sigma_{ij}^{(1)} \left(\frac{\partial^2 u_i^{(2)}}{\partial x_j \partial x_1} - \frac{\partial \varepsilon_{ij}^{(2)}}{\partial x_1} \right) + D_j^{(1)} \left(\frac{\partial^2 \phi^{(2)}}{\partial x_j \partial x_1} + \frac{\partial E_j^{(2)}}{\partial x_1} \right) - \varepsilon_{ij}^{(1)} \frac{\partial C_{ijkl}}{\partial x_1} \varepsilon_{kl}^{(2)} \\ + \left(E_n^{(1)} \frac{\partial e_{nkl}}{\partial x_1} \varepsilon_{kl}^{(2)} + E_n^{(2)} \frac{\partial e_{nkl}}{\partial x_1} \varepsilon_{kl}^{(1)} \right) + E_n^{(1)} \frac{\partial \kappa_{nm}}{\partial x_1} E_m^{(2)} \end{array} \right) q \ \mathrm{d}A, \tag{50}$$

is another modified interaction integral for non-homogeneous piezoelectric materials.

4.2.3. Method III – non-equilibrium formulation

This method entails the auxiliary displacement and electric potential given by Eqs. (13) and (14), and calculating the auxiliary strain and electric fields from the symmetric gradient of the auxiliary displacement field and the gradient of the auxiliary electric potential. The auxiliary stress and electrical displacement fields are computed using the same spatially varying elastic, piezoelectric and dielectric material tensors of the FGPM. In this approach, the auxiliary stress and electrical displacement fields does not satisfy equilibrium ($\partial \sigma_{ij}^{(2)}/\partial x_j \neq 0, \partial D_i^{(2)}/\partial x_i \neq 0$); however, the auxiliary strain and electric fields are compatible with the auxiliary displacement field and electric potential ($\varepsilon_{ij}^{(2)} = (\partial u_i^{(2)}/\partial x_j + \partial u_j^{(2)}/\partial x_i)/2, E_i^{(2)} = -\partial \phi^{(2)}/\partial x_i$). If the auxiliary field does not satisfy equilibrium, extra terms that will arise due to violation of equilibrium condition should be taken into account while evaluating the interaction integral. Therefore, this method also introduces additional terms to the resulting interaction integral.

Following similar considerations, but using only equilibrium condition in the auxiliary state, Eq. (41) can also be simplified to

$$\widetilde{J}^{(S)} = \int_A \left((\sigma_{ij}^{(1)} + \sigma_{ij}^{(2)}) \frac{\partial (u_i^{(1)} + u_i^{(2)})}{\partial x_1} + (D_j^{(1)} + D_j^{(2)}) \frac{\partial (\phi^{(1)} + \phi^{(2)})}{\partial x_1} - (H^{(1)} + H^{(2)} + H^{(1,2)}) \delta_{1j} \right) \frac{\partial q}{\partial x_j} \mathrm{d}A + \int_A \left(\begin{array}{l} \frac{\partial \sigma_{ij}^{(2)}}{\partial x_j} \frac{\partial (u_i^{(1)} + u_i^{(2)})}{\partial x_1} + \frac{\partial D_j^{(2)}}{\partial x_j} \frac{\partial (\phi^{(1)} + \phi^{(2)})}{\partial x_1} \\ - \frac{1}{2} (\varepsilon_{ij}^{(1)} + \varepsilon_{ij}^{(2)}) \frac{\partial C_{ijkl}}{\partial x_1} (\varepsilon_{kl}^{(1)} + \varepsilon_{kl}^{(2)}) + (E_n^{(1)} + E_n^{(2)}) \frac{\partial e_{nkl}}{\partial x_1} (\varepsilon_{kl}^{(1)} + \varepsilon_{kl}^{(2)}) \\ + \frac{1}{2} (E_n^{(1)} + E_n^{(2)}) \frac{\partial \kappa_{nm}}{\partial x_1} (E_m^{(1)} + E_m^{(2)}) \end{array} \right) q \ \mathrm{d}A \tag{51}$$

Comparing Eqs. (47) and (43)

$$\widetilde{J}^{(1)} = \int_A \left(\sigma_{ij}^{(1)} \frac{\partial u_i^{(1)}}{\partial x_1} + D_j^{(1)} \frac{\partial \phi^{(1)}}{\partial x_1} - H^{(1)} \delta_{1j} \right) \frac{\partial q}{\partial x_j} \mathrm{d}A - \int_A \left(\frac{1}{2} \varepsilon_{ij}^{(1)} \frac{\partial C_{ijkl}}{\partial x_1} \varepsilon_{kl}^{(1)} - \varepsilon_{kl}^{(1)} \frac{\partial e_{nkl}}{\partial x_1} E_n^{(1)} - \frac{1}{2} E_n^{(1)} \frac{\partial \kappa_{nm}}{\partial x_1} E_m^{(1)} \right) q \ \mathrm{d}A, \tag{52}$$

$$\widetilde{J}^{(2)} = \int_A \left(\sigma_{ij}^{(2)} \frac{\partial u_i^{(2)}}{\partial x_1} + D_j^{(2)} \frac{\partial \phi^{(2)}}{\partial x_1} - H^{(2)} \delta_{1j} \right) \frac{\partial q}{\partial x_j} \mathrm{d}A + \int_A \left(\begin{array}{l} \frac{\partial \sigma_{ij}^{(2)}}{\partial x_j} \frac{\partial u_i^{(2)}}{\partial x_1} + \frac{\partial D_j^{(2)}}{\partial x_j} \frac{\partial \phi^{(2)}}{\partial x_1} \\ - \frac{1}{2} \varepsilon_{ij}^{(2)} \frac{\partial C_{ijkl}}{\partial x_1} \varepsilon_{kl}^{(2)} + E_n^{(2)} \frac{\partial e_{nkl}}{\partial x_1} \varepsilon_{kl}^{(2)} + \frac{1}{2} E_n^{(2)} \frac{\partial \kappa_{nm}}{\partial x_1} E_m^{(2)} \end{array} \right) q \ \mathrm{d}A, \tag{53}$$

are the electromechanical $\widetilde{J}$-integrals for states 1 and 2, respectively, and

$$\widetilde{M}^{(1,2)} = \int_A \left(\sigma_{ij}^{(1)} \frac{\partial u_i^{(2)}}{\partial x_1} + \sigma_{ij}^{(2)} \frac{\partial u_i^{(1)}}{\partial x_1} + D_j^{(1)} \frac{\partial \phi^{(2)}}{\partial x_1} + D_j^{(2)} \frac{\partial \phi^{(1)}}{\partial x_1} - H^{(1,2)} \delta_{1j} \right) \frac{\partial q}{\partial x_j} \mathrm{d}A + \int_A \left(\begin{array}{c} \frac{\partial \sigma_{ij}^{(2)}}{\partial x_j} \frac{\partial u_i^{(1)}}{\partial x_1} + \frac{\partial D_j^{(2)}}{\partial x_j} \frac{\partial \phi^{(1)}}{\partial x_1} - \varepsilon_{ij}^{(1)} \frac{\partial C_{ijkl}}{\partial x_1} \varepsilon_{kl}^{(2)} \\ + \left(E_n^{(1)} \frac{\partial e_{nkl}}{\partial x_1} \varepsilon_{kl}^{(2)} + E_n^{(2)} \frac{\partial e_{nkl}}{\partial x_1} \varepsilon_{kl}^{(1)} \right) + E_n^{(1)} \frac{\partial \kappa_{nm}}{\partial x_1} E_m^{(2)} \end{array} \right) q \ \mathrm{d}A \tag{54}$$

is another modified interaction integral for non-homogeneous piezoelectric materials.

Note, that for homogeneous piezoelectric materials, regardless of how the auxiliary field is defined, the $\widetilde{J}^{(1)}, \widetilde{J}^{(2)},$ and $\widetilde{M}^{(1,2)}$ integrals in methods I–III degenerate to their corresponding homogeneous solutions, as expected.

4.2.4. Proof of existence of interaction integral for FGPMs

Eqs. (46), (50) and (54) contains the second integral involving extra terms due to material non-homogeneity. The existence of the second integral in Eqs. (46), (50) and (54), as the limit $r \to 0$ is proved below. The material properties, such as C_{ijks}, e_{sij}, κ_{is}, must be continuous and differentiable functions, and thus can be written as

$$C_{ijks}(r,\theta) = C_{ijks}^{*} + r C_{ijks}^{(1)}(\theta) + \frac{r^2}{2} C_{ijks}^{(2)}(\theta) + \mathrm{O}(r^3) + \cdots, \tag{55}$$

$$e_{sij}(r,\theta) = e_{sij}^{*} + r e_{sij}^{(1)}(\theta) + \frac{r^2}{2} e_{sij}^{(2)}(\theta) + \mathrm{O}(r^3) + \cdots, \tag{56}$$

$$\kappa_{is}(r,\theta) = \kappa_{is}^{*} + r \kappa_{is}^{(1)}(\theta) + \frac{r^2}{2} \kappa_{is}^{(2)}(\theta) + \mathrm{O}(r^3) + \cdots, \tag{57}$$

where $C^*_{ijks}, e^*_{sij}, \kappa^*_{is}$ are the local material data at the crack tip, $\boldsymbol{x}^*$, and $C^{(n)}_{ijks}(\theta)$, $e^{(n)}_{sij}(\theta)$, and $\kappa^{(n)}_{is}(\theta)$ with $n = 1, 2, \ldots$ are angular functions. Hence, spatial derivatives of the material properties, C_{ijks}, e_{sij}, h_{sij}, κ_{is}, β_{is}, γ_{is}, are bounded at the crack tip, i.e., $C_{ijks,1}$, $e_{sij,1}$, $h_{sij,1}$, $\kappa_{is,1}$, $\beta_{is,1}$ and $\gamma_{is,1}$ are $O(r^{\alpha})$ with $\alpha \geqslant 0$. In the limit $r \to 0$ the integrand of the second integral in Eq. (46)

$$\begin{aligned}
&\lim_{r\to 0}\left[\frac{1}{2}\begin{pmatrix}\sigma^{(1)}_{ij}\frac{\partial\varepsilon^{(2)}_{ij}}{\partial x_1}-\frac{\partial\sigma^{(1)}_{ij}}{\partial x_1}\varepsilon^{(2)}_{ij}+\sigma^{(2)}_{ij}\frac{\partial\varepsilon^{(1)}_{ij}}{\partial x_1}-\frac{\partial\sigma^{(2)}_{ij}}{\partial x_1}\varepsilon^{(1)}_{ij}\\ -D^{(1)}_j\frac{\partial E^{(2)}_j}{\partial x_1}+\frac{\partial D^{(1)}_j}{\partial x_1}E^{(2)}_j-D^{(2)}_j\frac{\partial E^{(1)}_j}{\partial x_1}+\frac{\partial D^{(2)}_j}{\partial x_1}E^{(1)}_j\end{pmatrix}q\mathrm{d}A\right].\\
&=\lim_{r\to 0}\left[\frac{1}{2}\begin{pmatrix}\sigma^{(1)}_{ij}\frac{\partial\varepsilon^{(2)}_{ij}}{\partial x_1}-\frac{\partial\sigma^{(1)}_{ij}}{\partial x_1}\varepsilon^{(2)}_{ij}+\sigma^{(2)}_{ij}\frac{\partial\varepsilon^{(1)}_{ij}}{\partial x_1}-\frac{\partial\sigma^{(2)}_{ij}}{\partial x_1}\varepsilon^{(1)}_{ij}\\ -D^{(1)}_j\frac{\partial E^{(2)}_j}{\partial x_1}+\frac{\partial D^{(1)}_j}{\partial x_1}E^{(2)}_j-D^{(2)}_j\frac{\partial E^{(1)}_j}{\partial x_1}+\frac{\partial D^{(2)}_j}{\partial x_1}E^{(1)}_j\end{pmatrix}qr\mathrm{d}r\mathrm{d}\theta\right]=\lim_{r\to 0}\left[\mathrm{O}\left(r^{-\frac{1}{2}}\right)\mathrm{O}\left(r^{-\frac{3}{2}}\right)qr\mathrm{d}r\mathrm{d}\theta\right]\\
&=\lim_{r\to 0}\left[\mathrm{O}(r^{-1})qr\mathrm{d}r\mathrm{d}\theta\right]=0.
\end{aligned}\tag{58}$$

In Eq. (50), the incompatibility terms in the integrand of the second integral

$$\left(\sigma^{(1)}_{ij}\left(\frac{\partial^2 u^{(2)}_i}{\partial x_j\partial x_1}-\frac{\partial\varepsilon^{(2)}_{ij}}{\partial x_1}\right)+D^{(1)}_j\left(\frac{\partial^2\phi^{(2)}}{\partial x_j\partial x_1}+\frac{\partial E^{(2)}_j}{\partial x_1}\right)\right)q\mathrm{d}A\tag{59}$$

naturally vanish because the auxiliary fields are compatible very near the crack tip (asymptotically). Rest of the terms in the integrand of the second integral of Eq. (50) in the limit $r \to 0$ becomes

$$\begin{aligned}
&\lim_{r\to 0}\left[\left(-\varepsilon^{(1)}_{ij}\frac{\partial C_{ijkl}}{\partial x_1}\varepsilon^{(2)}_{kl}+\left(E^{(1)}_n\frac{\partial e_{nkl}}{\partial x_1}\varepsilon^{(2)}_{kl}+E^{(2)}_n\frac{\partial e_{nkl}}{\partial x_1}\varepsilon^{(1)}_{kl}\right)+E^{(1)}_n\frac{\partial\kappa_{nm}}{\partial x_1}E^{(2)}_m\right)q\mathrm{d}A\right]\\
&=\lim_{r\to 0}\left[\left(-\varepsilon^{(1)}_{ij}\frac{\partial C_{ijkl}}{\partial x_1}\varepsilon^{(2)}_{kl}+\left(E^{(1)}_n\frac{\partial e_{nkl}}{\partial x_1}\varepsilon^{(2)}_{kl}+E^{(2)}_n\frac{\partial e_{nkl}}{\partial x_1}\varepsilon^{(1)}_{kl}\right)+E^{(1)}_n\frac{\partial\kappa_{nm}}{\partial x_1}E^{(2)}_m\right)qr\mathrm{d}r\mathrm{d}\theta\right]\\
&=\lim_{r\to 0}\left[\mathrm{O}\left(r^{-\frac{1}{2}}\right)\mathrm{O}(r^{\alpha})\mathrm{O}\left(r^{-\frac{1}{2}}\right)qr\mathrm{d}r\mathrm{d}\theta\right]=\lim_{r\to 0}\left[\mathrm{O}(r^{\alpha})q\mathrm{d}r\mathrm{d}\theta\right]=0.
\end{aligned}\tag{60}$$

In Eq. (54), the non-equilibrium terms in the integrand of the second integral, as the limit $r \to 0$ becomes

$$\begin{aligned}
\lim_{r\to 0}\left[\left(\frac{\partial\sigma^{(2)}_{ij}}{\partial x_j}\frac{\partial u^{(1)}_i}{\partial x_1}+\frac{\partial D^{(2)}_j}{\partial x_j}\frac{\partial\phi^{(1)}}{\partial x_1}\right)q\mathrm{d}A\right]&=\lim_{r\to 0}\left[\left(\frac{\partial\sigma^{(2)}_{ij}}{\partial x_j}\frac{\partial u^{(1)}_i}{\partial x_1}+\frac{\partial D^{(2)}_j}{\partial x_j}\frac{\partial\phi^{(1)}}{\partial x_1}\right)qr\mathrm{d}r\mathrm{d}\theta\right]\\
&=\lim_{r\to 0}\left[\mathrm{O}\left(r^{\alpha-\frac{1}{2}}\right)\mathrm{O}\left(r^{-\frac{1}{2}}\right)qr\mathrm{d}r\mathrm{d}\theta\right]=\lim_{r\to 0}\left[\mathrm{O}(r^{\alpha})q\mathrm{d}r\mathrm{d}\theta\right]=0.
\end{aligned}\tag{61}$$

In the limit $r \to 0$ rest of the terms in the second integral of Eq. (54) becomes as given in Eq. (60). Thus all the proposed interaction integrals for non-homogeneous piezoelectric materials in Eqs. (46), (50) and (54) are well posed as the limit $r \to 0$ exists.

4.2.5. Numerical aspects in computation of interaction integrals

For numerical computation of the proposed interaction integrals in the crack coordinate system, first all the state 1 quantities corresponding to the *actual* state for the given boundary conditions are evaluated in the material coordinate system and then transformed to the crack coordinate system. All the state 2 quantities corresponding to an *auxiliary* state are evaluated in the crack coordinate system using the transformed material property tensors C_{ijks}, e_{iks} and κ_{is}, from the material coordinate system to the crack coordinate system. The derivatives of material property tensors C_{ijks}, e_{iks} and κ_{is}, can be obtained by means of shape function derivatives.

4.2.6. Intensity factors evaluation

For linear piezoelectric solids, the electromechanical $\widetilde{J}$-integral also represents the energy release rate and, hence for two-dimensional case

$$\widetilde{J}=\frac{1}{2}K^2_{\mathrm{II}}Y^*_{11}+\frac{1}{2}K^2_{\mathrm{I}}Y^*_{22}+\frac{1}{2}K^2_{\mathrm{IV}}Y^*_{44}+K_{\mathrm{I}}K_{\mathrm{II}}Y^*_{12}+K_{\mathrm{II}}K_{\mathrm{IV}}Y^*_{14}+K_{\mathrm{I}}K_{\mathrm{IV}}Y^*_{24},\tag{62}$$

where $Y^*_{MN}=Y_{MN}(\boldsymbol{x}^*)$ being the components of the (4×4) generalized Irwin matrix, $\boldsymbol{Y}$ is evaluated with the local material data at the crack tip, $\boldsymbol{x}^*$. Regardless of how the auxiliary fields are defined, Eq. (62) applied to states 1, 2, and S yields

$$\widetilde{J}^{(1)}=\frac{1}{2}K^{(1)2}_{\mathrm{II}}Y^*_{11}+\frac{1}{2}K^{(1)2}_{\mathrm{I}}Y^*_{22}+\frac{1}{2}K^{(1)2}_{\mathrm{IV}}Y^*_{44}+K^{(1)}_{\mathrm{I}}K^{(1)}_{\mathrm{II}}Y^*_{12}+K^{(1)}_{\mathrm{II}}K^{(1)}_{\mathrm{IV}}Y^*_{14}+K^{(1)}_{\mathrm{I}}K^{(1)}_{\mathrm{IV}}Y^*_{24},\tag{63}$$

$$\widetilde{J}^{(2)}=\frac{1}{2}K^{(2)2}_{\mathrm{II}}Y^*_{11}+\frac{1}{2}K^{(2)2}_{\mathrm{I}}Y^*_{22}+\frac{1}{2}K^{(2)2}_{\mathrm{IV}}Y^*_{44}+K^{(2)}_{\mathrm{I}}K^{(2)}_{\mathrm{II}}Y^*_{12}+K^{(2)}_{\mathrm{II}}K^{(2)}_{\mathrm{IV}}Y^*_{14}+K^{(2)}_{\mathrm{I}}K^{(2)}_{\mathrm{IV}}Y^*_{24},\tag{64}$$

and

$$\widetilde{J}^{(S)} = \widetilde{J}^{(1)} + \widetilde{J}^{(2)} + K_{\mathrm{II}}^{(1)}K_{\mathrm{II}}^{(2)}Y_{11}^{*} + K_{\mathrm{I}}^{(1)}K_{\mathrm{I}}^{(2)}Y_{22}^{*} + K_{\mathrm{IV}}^{(1)}K_{\mathrm{IV}}^{(2)}Y_{44}^{*} + \left(K_{\mathrm{I}}^{(1)}K_{\mathrm{II}}^{(2)} + K_{\mathrm{II}}^{(1)}K_{\mathrm{I}}^{(2)}\right)Y_{12}^{*} + \left(K_{\mathrm{II}}^{(1)}K_{\mathrm{IV}}^{(2)} + K_{\mathrm{IV}}^{(1)}K_{\mathrm{II}}^{(2)}\right)Y_{14}^{*} + \left(K_{\mathrm{I}}^{(1)}K_{\mathrm{IV}}^{(2)} + K_{\mathrm{IV}}^{(1)}K_{\mathrm{I}}^{(2)}\right)Y_{24}^{*}. \tag{65}$$

Comparing Eq. (43) with Eq. (65)

$$\widetilde{M}^{(1,2)} = K_{\mathrm{II}}^{(1)}K_{\mathrm{II}}^{(2)}Y_{11}^{*} + K_{\mathrm{I}}^{(1)}K_{\mathrm{I}}^{(2)}Y_{22}^{*} + K_{\mathrm{IV}}^{(1)}K_{\mathrm{IV}}^{(2)}Y_{44}^{*} + (K_{\mathrm{I}}^{(1)}K_{\mathrm{II}}^{(2)} + K_{\mathrm{II}}^{(1)}K_{\mathrm{I}}^{(2)})Y_{12}^{*} + (K_{\mathrm{II}}^{(1)}K_{\mathrm{IV}}^{(2)} + K_{\mathrm{IV}}^{(1)}K_{\mathrm{II}}^{(2)})Y_{14}^{*} + (K_{\mathrm{I}}^{(1)}K_{\mathrm{IV}}^{(2)} + K_{\mathrm{IV}}^{(1)}K_{\mathrm{I}}^{(2)})Y_{24}^{*}. \tag{66}$$

Following a similar procedure and judiciously choosing the intensity of the auxiliary state as described earlier, the SIFs and EDIF for non-homogenous piezoelectric materials can be obtained by solving the following three simultaneous Eqs. (67)–(69)

$$\widetilde{M}^{(1,\mathrm{I})} = K_{\mathrm{I}}^{(1)}Y_{22}^{*} + K_{\mathrm{II}}^{(1)}Y_{12}^{*} + K_{\mathrm{IV}}^{(1)}Y_{24}^{*}, \tag{67}$$

$$\widetilde{M}^{(1,II)} = K_{\mathrm{I}}^{(1)}Y_{12}^{*} + K_{\mathrm{II}}^{(1)}Y_{11}^{*} + K_{\mathrm{IV}}^{(1)}Y_{14}^{*}, \tag{68}$$

and

$$\widetilde{M}^{(1,\mathrm{IV})} = K_{\mathrm{I}}^{(1)}Y_{24}^{*} + K_{\mathrm{II}}^{(1)}Y_{14}^{*} + K_{\mathrm{IV}}^{(1)}Y_{44}^{*}. \tag{69}$$

In Eqs. (67)–(69) $\widetilde{M}^{(1,\mathrm{I})}$, $\widetilde{M}^{(1,\mathrm{II})}$ and $\widetilde{M}^{(1,\mathrm{IV})}$ are three modified interaction integrals for the three fracture opening modes I, II, and IV, respectively, and can be evaluated using any of the Eqs. (46), (50) and (54). All the three methods are used in performing numerical calculations, to be presented in a forthcoming section.

Note, Eqs. (67)–(69) are the result of a simple generalization of the interaction integral method for calculating the SIFs and EDIF in linear homogenous piezoelectric materials. When there is no spatial variation in the material properties C_{ijks}, e_{sij}, κ_{is}, $\widetilde{M}^{(1,2)} = M^{(1,2)}$. Consequently, Eqs. (67)–(69) degenerate into Eqs. (37)–(39), as expected.

5. Numerical examples

In this study, accuracy of the predicted SIFs and EDIF using the interaction integrals based on three formulations is investigated by comparing with those obtained by using displacement extrapolation method (DEM). The SIFs and EDIF in piezoelectric materials can be evaluated using DEM with the help of discontinuity of displacements and electric potential across the crack faces as follows:

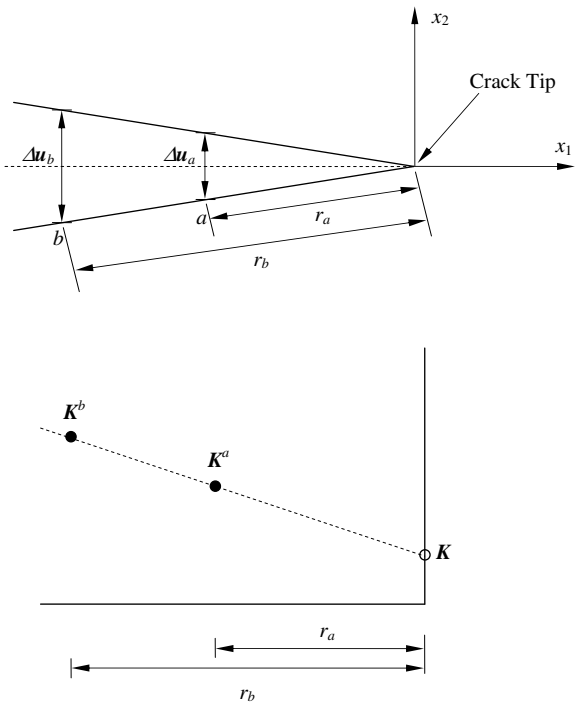

Fig. 2. Displacement extrapolation method.

$$\boldsymbol{K} = \lim_{r\to 0} \sqrt{\frac{\pi}{8r}} \boldsymbol{Y}^{-1} \begin{Bmatrix} \Delta u_1 \\ \Delta u_2 \\ \Delta u_3 \\ \Delta \phi \end{Bmatrix}. \tag{70}$$

In finite element (FE) calculations, the relative displacements and electric potential between two nodes on the crack surface are used for determination of the SIFs and EDIF. Namely, from displacements and electric potential at a node i on the crack surface located at a distance r_i from the crack tip, intensity factors $\mathbf{K}^i$ are calculated using

$$\boldsymbol{K}^i = \sqrt{\frac{\pi}{8r_i}} \boldsymbol{Y}^{-1} \begin{Bmatrix} \Delta u_1 \\ \Delta u_2 \\ \Delta u_3 \\ \Delta \phi \end{Bmatrix}. \tag{71}$$

As shown in Fig. 2, intensity factors values at two points 'a' and 'b' near the crack tip are calculated by Eq. (71) and extrapolated so as to obtain the SIFs and EDIF, as follows:

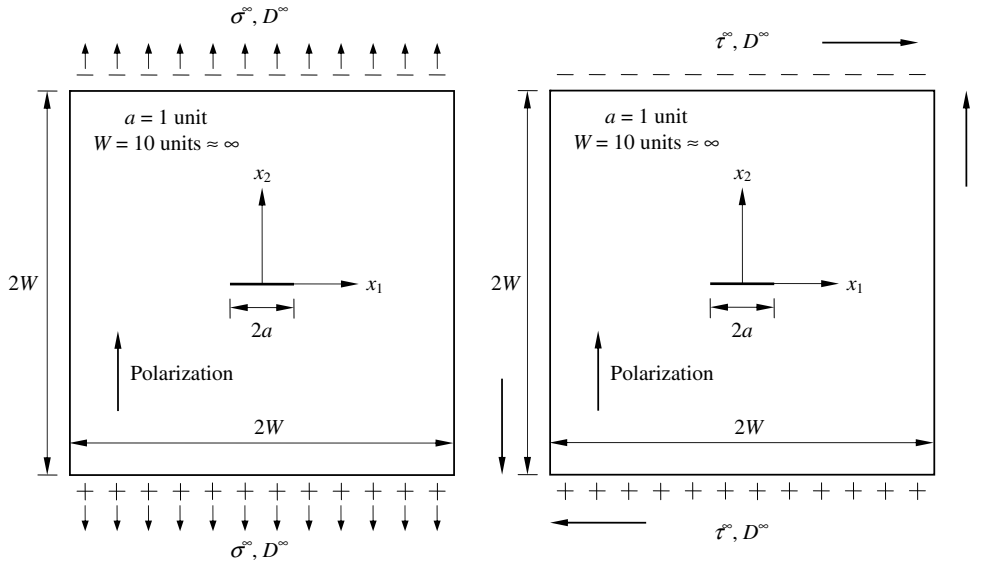

(a) Geometry, and loads under far-field normal load σ^∞ and far-field electrical displacement load D^∞

(b) Geometry, and loads under far-field shear load τ^∞ and far-field electrical displacement load D^∞

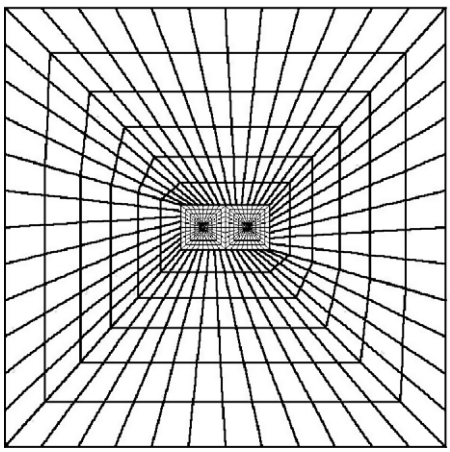

(c) FEM discretization (2416 nodes, 736 8-noded quadrilateral elements, and 64 focused quarter-point 6-noded triangular elements)

Fig. 3. Finite horizontal crack in an infinite medium (example 1).

$$\boldsymbol{K} = \frac{r_a \boldsymbol{K}^b - r_b \boldsymbol{K}^a}{r_a - r_b}, \tag{72}$$

where r_a and r_b are respectively the distance of two points 'a' and 'b' from the crack tip. For non-homogeneous piezoelectric materials generalized Irwin matrix, $\boldsymbol{Y}$ in Eq. (71) has to be evaluated with the local material data at the crack tip, $\boldsymbol{x}^*$.

In the two numerical examples presented below, the material properties are assumed to be one-dimensionally dependent as

$$\begin{matrix}(C_{11}, C_{22}, C_{12}, C_{13}, C_{44}, e_{21}, e_{22}, e_{16}, \kappa_{11}, \kappa_{22})(\boldsymbol{x}) = \\ (C_{110}, C_{220}, C_{120}, C_{130}, C_{440}, e_{210}, e_{220}, e_{160}, \kappa_{110}, \kappa_{220}) \exp(\eta x_1)\end{matrix}, -W \leqslant x_1 \leqslant W, \tag{73}$$

where η is a non-homogeneity parameter that controls the variation of material properties. In numerical examples $\eta a = -0.5$, -0.25, -0.125, 0, 0.125, 0.25, and 0.5 are considered, which corresponds to 0.000045401, 0.0067, 0.0821, 1, 12.185, 148.413, and 22026.5 respectively as the ratio of the material properties at left edge to that at right edge of the domain, for the geometric configurations adopted in numerical examples with $W = 10$ and $a = 1$. The following material constants are adopted in the two numerical examples presented:

$$\begin{matrix} C_{110} = 12.6 \times 10^{10}\ \text{Pa} & C_{220} = 11.7 \times 10^{10}\ \text{Pa} & C_{120} = 5.3 \times 10^{10}\ \text{Pa} \\ C_{130} = 5.5 \times 10^{10}\ \text{Pa} & C_{440} = 3.53 \times 10^{10}\ \text{Pa} & \\ e_{210} = -6.5 \times 10^{9}\ \text{N/(GVm)} & e_{220} = 23.3 \times 10^{9}\ \text{N/(GVm)} & e_{160} = 17 \times 10^{9}\ \text{N/(GVm)} \\ \kappa_{110} = 15.1 \times 10^{9}\ \text{N/(GV)}^2 & \kappa_{220} = 13 \times 10^{9}\ \text{N/(GV)}^2 & \end{matrix}. \tag{74}$$

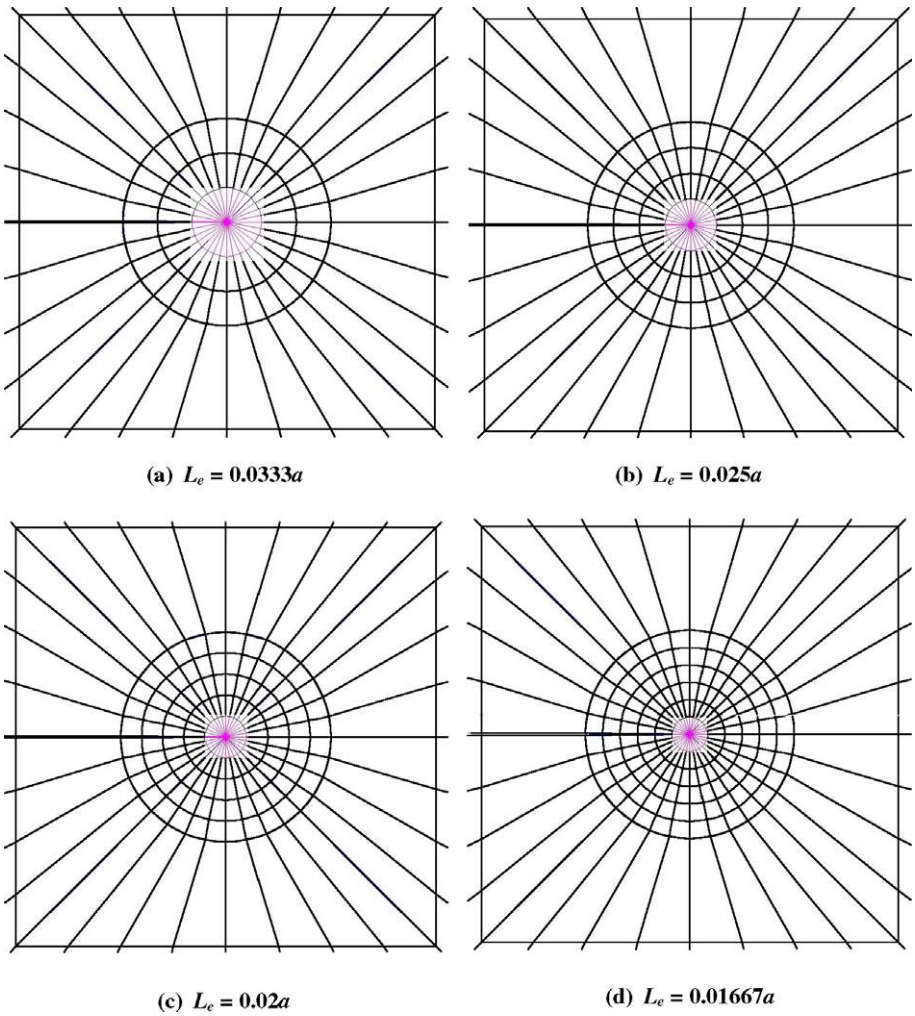

Fig. 4. Mesh refinements around the crack tip for finite horizontal crack in an infinite medium (example 1).

In the numerical examples studied the loading combination parameter defined as $\lambda = D^{\infty}c_{330}/(\sigma^{\infty}e_{330})$ or $\lambda = D^{\infty}c_{330}/(\tau^{\infty}e_{330})$ is used to reflect the combination between the far-field normal load σ^{∞} and the far-field electrical displacement load D^{∞} or the combination between the far-field shear load τ^{∞} and the far-field electrical displacement load D^{∞}. The loading combination parameter $\lambda = 0$, corresponds to the case of far-field electrical displacement load $D^{\infty} = 0$. An impermeable crack in an infinite medium is considered in all numerical examples presented. Obviously, a FE model cannot represent the infinite domain, but as long as the ratio a/W is kept relatively small (e.g., $a/W \leqslant 1/10$), the infinite medium approximation is acceptable.

5.1. Example 1: finite horizontal crack in an infinite medium

The geometric configuration and the loads considered in this study are shown in Fig. 3(a) and (b). Two types of loading combinations are studied: (1) type 1: the far-field normal load σ^{∞} and the far-field electrical displacement load D^{∞}; (2) type 2: the far-field shear load τ^{∞} and the far-field electrical displacement load D^{∞}. The poling direction is assumed to be oriented perpendicular to the crack. FE model adopted for the evaluation of intensity factors using the interaction integrals based on the proposed three formulations (in Eqs. (46), (50) and (54)) involves 2416 nodes, 736 eight-noded quadrilateral elements, and 64 focused quarter-point six-noded triangular elements, as shown in Fig. 3(c). The SIFs and EDIF are also evaluated using DEM.

For the evaluation of intensity factors using DEM r_a and r_b are taken to be equal to $L_e/4$ and L_e respectively, where L_e is the length of six-noded triangular quarter-point element edge containing 1/4-point node. Before comparing intensity factors obtained using the proposed interaction integrals with the values obtained using DEM, convergence of the values obtained using the later method, for different values of $L_e = 0.0333a$, $0.025a$, $0.02a$, $0.01667a$ is verified by using four different mesh refinements around the crack tip with FE discretizations involving 2416 nodes, 2612 nodes, 2808 nodes, and 3004 nodes, respectively over the entire domain. The magnified view of mesh refinements around the crack tip for these four FE discretizations are shown in Fig. 4(a)–(d). Fig. 5(a) and (b) show the convergence of the normalized mode-I SIF $K_{\mathrm{I}}/(\sigma^{\infty}\sqrt{\pi a})$, and the normalized EDIF $K_{\mathrm{IV}}/(D^{\infty}\sqrt{\pi a})$ evaluated at the right crack tip, with respect to L_e/a, under type 1 loading combination for

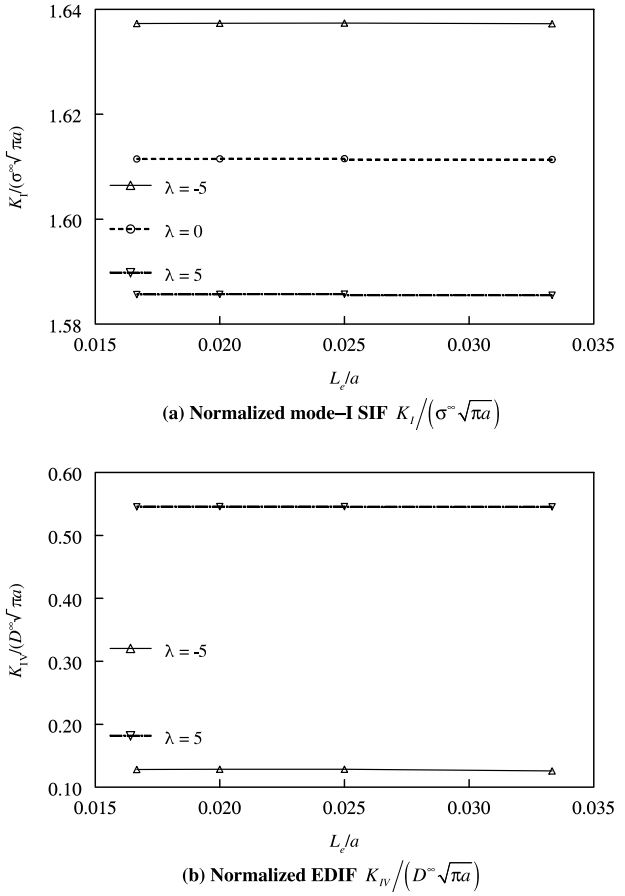

Fig. 5. Convergence with respect to L_e/a under type 1 loading combination (example 1).

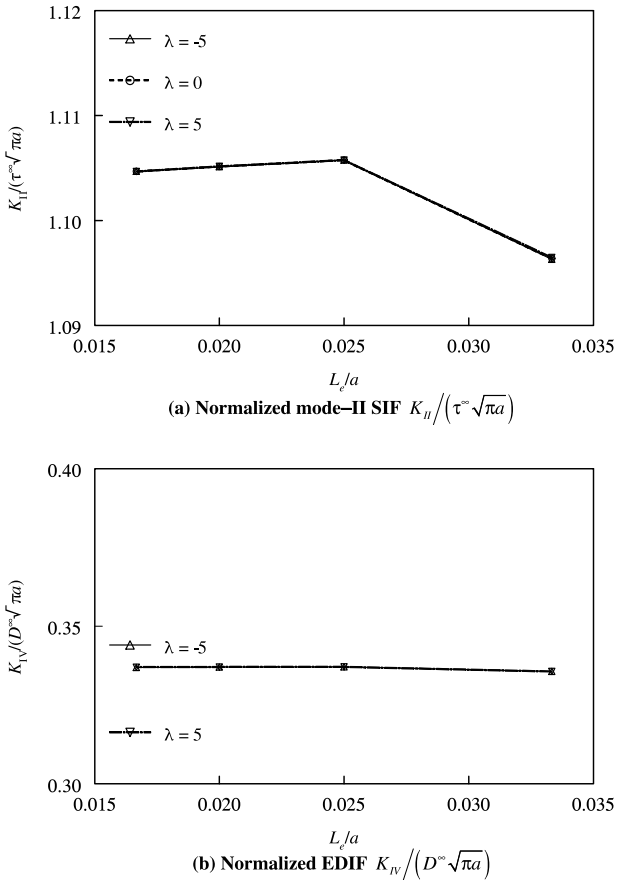

Fig. 6. Convergence with respect to L_e/a under type 2 loading combination (example 1).

Table 1
Normalized mode-I stress intensity factor $K_I/(\sigma^{\infty}\sqrt{\pi a})$ under far-field normal load σ^{∞} and far-field electrical displacement load D^{∞} (example 1)

ηa	$\lambda = -5$				$\lambda = 0$				$\lambda = 5$			
	Method-I	Method-II	Method-III	DEM	Method-I	Method-II	Method-III	DEM	Method-I	Method-II	Method-III	DEM
−0.5	1.019055	1.019016	1.019010	1.021536	1.058626	1.058601	1.058594	1.061156	1.098198	1.098186	1.098178	1.100775
−0.25	1.276499	1.276472	1.276467	1.279606	1.218011	1.217999	1.217993	1.220860	1.159523	1.159525	1.159519	1.162113
−0.125	1.127687	1.127672	1.127669	1.130491	1.093417	1.093411	1.093409	1.095962	1.059146	1.059149	1.059148	1.061433
0	1.012148	1.012148	1.012148	1.014673	1.012222	1.012222	1.012222	1.014542	1.012297	1.012297	1.012297	1.014412
0.125	1.243388	1.243404	1.243407	1.246290	1.185416	1.185421	1.185426	1.188021	1.127444	1.127438	1.127445	1.129752
0.25	1.607416	1.607439	1.607446	1.610914	1.482584	1.482592	1.482599	1.485704	1.357753	1.357745	1.357752	1.360493
0.5	1.634073	1.634090	1.634104	1.637320	1.608359	1.608361	1.608376	1.611499	1.582646	1.582632	1.582647	1.585679

Table 2
Normalized electric displacement intensity factor $K_{IV}/(D^{\infty}\sqrt{\pi a})$ under far-field normal load σ^{∞} and far-field electrical displacement load D^{∞} (example 1)

ηa	$\lambda = -5$				$\lambda = 5$			
	Method-I	Method-II	Method-III	DEM	Method-I	Method-II	Method-III	DEM
−0.5	0.091165	0.091076	0.091166	0.089083	0.386365	0.386378	0.386390	0.386608
−0.25	0.391283	0.391194	0.391287	0.387324	0.719800	0.719769	0.719813	0.718707
−0.125	0.749049	0.748987	0.749053	0.743674	0.895752	0.895722	0.895757	0.893672
0	1.002041	1.002041	1.002041	0.995632	1.006458	1.006458	1.006458	1.003751
0.125	0.868655	0.868732	0.868653	0.862348	0.991505	0.991544	0.991501	0.989027
0.25	0.516549	0.516675	0.516545	0.511144	0.875067	0.875127	0.875065	0.873510
0.5	0.132172	0.132332	0.132161	0.128452	0.545319	0.545346	0.545325	0.545686

Table 3
Normalized mode-II stress intensity factor $K_{II}/(\tau^{\infty}\sqrt{\pi a})$ under far-field shear load τ^{∞} and far-field electrical displacement load D^{∞} (Example 1)

ηa	$\lambda = -5$				$\lambda = 0$				$\lambda = 5$			
	Method-I	Method-II	Method-III	DEM	Method-I	Method-II	Method-III	DEM	Method-I	Method-II	Method-III	DEM
−0.5	0.874329	0.874116	0.874245	0.868701	0.874252	0.874039	0.874291	0.866994	0.874176	0.873963	0.874336	0.865286
−0.25	0.942128	0.941981	0.942193	0.931194	0.942112	0.941966	0.942187	0.930947	0.942097	0.941950	0.942182	0.930701
−0.125	0.976353	0.976270	0.976389	0.982984	0.976349	0.976266	0.976388	0.978862	0.976345	0.976262	0.976387	0.974708
0	1.008864	1.008864	1.008864	0.998522	1.008866	1.008866	1.008866	0.998353	1.008867	1.008867	1.008867	0.998185
0.125	1.039821	1.039923	1.039784	1.028499	1.039820	1.039923	1.039782	1.028506	1.039820	1.039922	1.039780	1.028511
0.25	1.068013	1.068236	1.067946	1.055827	1.068026	1.068249	1.067955	1.055908	1.068039	1.068261	1.067965	1.055989
0.5	1.118331	1.118846	1.118174	1.105121	1.118350	1.118864	1.118194	1.105146	1.118368	1.118883	1.118213	1.105168

Table 4
Normalized electric displacement intensity factor $K_{IV}/(D^{\infty}\sqrt{\pi a})$ under far-field shear load τ^{∞} and far-field electrical displacement load D^{∞} (example 1)

ηa	$\lambda = -5$				$\lambda = 5$			
	Method-I	Method-II	Method-III	DEM	Method-I	Method-II	Method-III	DEM
−0.5	0.238827	0.238788	0.238839	0.237907	0.238704	0.238665	0.238716	0.237784
−0.25	0.555570	0.555510	0.555579	0.553044	0.555513	0.555453	0.555522	0.552987
−0.125	0.822419	0.822373	0.822423	0.818692	0.822382	0.822336	0.822387	0.818655
0	1.004262	1.004262	1.004262	0.999704	1.004237	1.004237	1.004237	0.999679
0.125	0.930092	0.930150	0.930089	0.925700	0.930068	0.930126	0.930065	0.925675
0.25	0.695819	0.695912	0.695816	0.692338	0.695797	0.695890	0.695794	0.692316
0.5	0.338735	0.338829	0.338733	0.337058	0.338756	0.338849	0.338753	0.337079

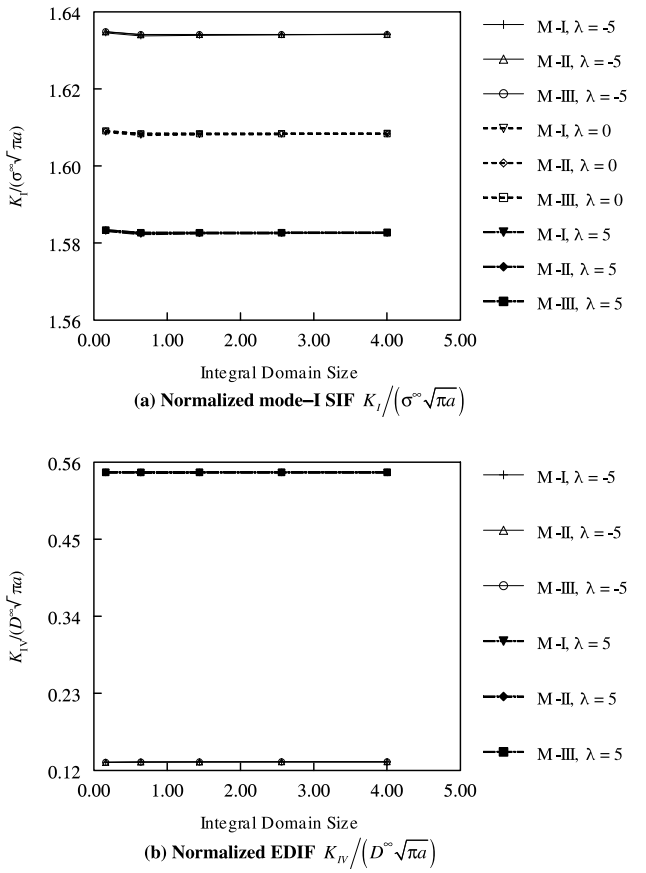

(a) Normalized mode–I SIF $K_I/\left(\sigma^{\infty}\sqrt{\pi a}\right)$

(b) Normalized EDIF $K_{IV}/\left(D^{\infty}\sqrt{\pi a}\right)$

Fig. 7. Integral domain dependence under Type 1 loading combination and $\eta a = 0.5$ (Example 1).

various values of λ and $\eta a = 0.5$. Similarly Fig. 6(a) and (b) show the convergence of the normalized mode-II SIF $K_{II}/(\tau^{\infty}\sqrt{\pi a})$, and the normalized EDIF $K_{IV}/(D^{\infty}\sqrt{\pi a})$ evaluated at the right crack tip with respect to L_e/a, under type 2 loading combination for various values of λ and $\eta a = 0.5$. It can be observed that convergence of intensity factors is achieved with $L_e = 0.02a$.

Intensity factors obtained using the proposed interaction integrals are compared with those obtained using DEM (with FE model involving 2808 nodes and $L_e = 0.02a$), which is presented in tabular form to facilitate comparison of the computed SIFs and EDIF by the three formulations to desired significant digit accuracy. Tables 1 and 2, show respectively the normalized mode-I SIF $K_I/(\sigma^{\infty}\sqrt{\pi a})$, and the normalized EDIF $K_{IV}/(D^{\infty}\sqrt{\pi a})$ evaluated at the right crack tip, under type 1 loading combination using methods I–III and DEM for various combinations of λ and ηa. A domain size of 1.6 units $\times$ 1.6 units is taken around the right crack tip to calculate the $\tilde{M}^{(1,2)}$-integral. It can be observed that irrespective of the values of λ and ηa all the three proposed interaction integrals predicted almost the same value of the same normalized intensity factors, which agrees well with those obtained using DEM. However, method I (constant constitutive tensor formulation) requires the derivatives of the actual stress and electrical displacement fields, which in turn requires second order derivatives of FE shape functions, which needs additional effort and also this requirement may introduce accuracy problems with C^0 elements. As, in the present study eight-noded quadrilateral elements, and six-noded triangular elements are adopted, all the three proposed interaction integral methods resulted in almost the same value of the normalized intensity factors to the significant digit accuracy considered.

Similarly, Tables 3 and 4, show respectively the normalized mode-II SIF $K_{II}/(\tau^{\infty}\sqrt{\pi a})$, and the normalized EDIF $K_{IV}/(D^{\infty}\sqrt{\pi a})$ evaluated at the right crack tip, under type 2 loading combination for various combinations of λ and ηa. Under type 1 loading combination, it can be observed from Tables 1 and 2 that the loading combination parameter λ has more influence on the normalized EDIF $K_{IV}/(D^{\infty}\sqrt{\pi a})$ than on the normalized mode-I SIF $K_I/(\sigma^{\infty}\sqrt{\pi a})$. When the magnitude of the applied electrical displacement load increases, its influence on $K_{IV}/(D^{\infty}\sqrt{\pi a})$ will decrease. This means that the mechanical load has insignificant effect on $K_{IV}/(D^{\infty}\sqrt{\pi a})$ under a strong electrical load. The current observations agree very well with those reported by Chen et al., 2003) based on analytical study. However, under type 2 loading combination, it can be observed from Tables 3 and 4 that the loading combination parameter λ has negligible influence on both the normalized mode-II SIF $K_{II}/(\tau^{\infty}\sqrt{\pi a})$, and the normalized EDIF $K_{IV}/(D^{\infty}\sqrt{\pi a})$.

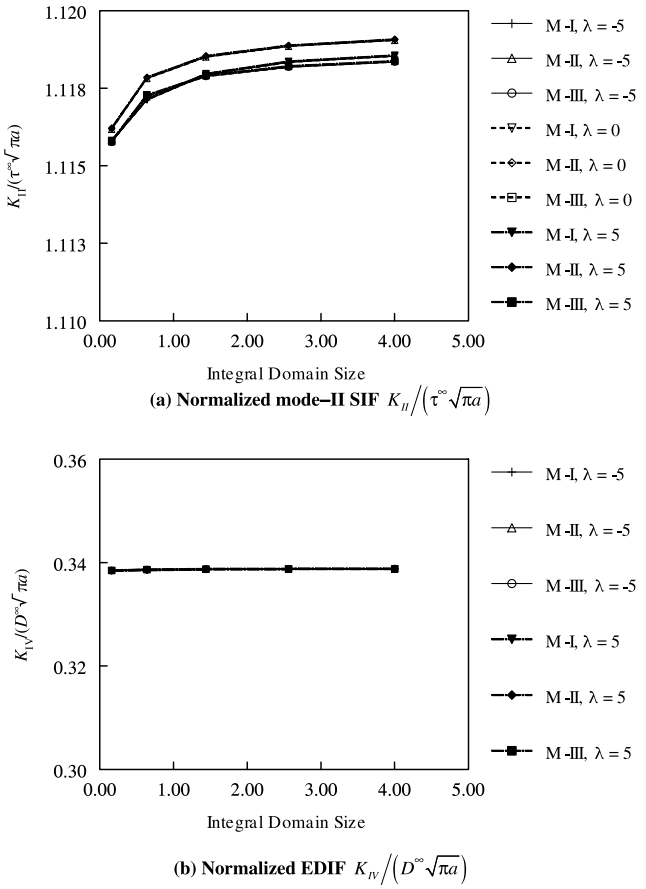

Fig. 8. Integral domain dependence under Type 2 loading combination and $\eta a = 0.5$ (Example 1).

The domain independence of intensity factors by the three proposed interaction integral methods is verified by employing the following five different integral domain sizes taken around the crack tip to calculate the $\tilde{M}^{(1,2)}$-integral: 0.4 units × 0.4 units, 0.8 units × 0.8 units, 1.2 units × 1.2 units, 1.6 units × 1.6 units, and 2.0 units × 2.0 units. Fig. 7(a) and (b) show the domain dependence of intensity factors of the normalized mode-I SIF $K_I/(\sigma^\infty\sqrt{\pi a})$, and the normalized EDIF $K_{IV}/(D^\infty\sqrt{\pi a})$ evaluated at the right crack tip, using methods I–III (M-I, M-II, M-III) with respect to various integral domain sizes, under type 1 loading combination for various values of λ and $\eta a = 0.5$. Similarly Fig. 8(a) and (b) show the domain dependence of the normalized mode-II SIF $K_{II}/(\tau^\infty\sqrt{\pi a})$, and the normalized EDIF $K_{IV}/(D^\infty\sqrt{\pi a})$ evaluated at the right crack tip, using methods I–III (M-I, M-II, M-III) with respect to various sizes of the integral domain, under type 2 loading combination for various values of λ and $\eta a = 0.5$. It can be observed that all the three proposed interaction integrals predicted domain independent solution with larger integral domains.

The significance of extra correction terms in the proposed interaction integrals for non-homogeneous piezoelectric materials (due to the non-homogeneous constitutive relation of the FGPM in constant constitutive tensor formulation; due to lack of compatibility in incompatibility formulation; and due to violation of equilibrium condition in non-equilibrium formulation), is studied using methods I–III with respect to different integral domain sizes, both under type 1 and 2 loading combinations for $\lambda = 5$ and $\eta a = 0.5$. Fig. 9(a) and (b) show the normalized mode-I SIF $K_I/(\sigma^\infty\sqrt{\pi a})$, and the normalized EDIF $K_{IV}/(D^\infty\sqrt{\pi a})$ evaluated at the right crack tip, using methods I–III without extra correction terms (M-I (NC), M-II (NC), M-III (NC)) and with extra correction terms (M-I (WC), M-II (WC), M-III (WC)) with respect to various integral domain sizes. Similarly Fig. 10(a) and (b) show the normalized mode-II SIF $K_{II}/(\tau^\infty\sqrt{\pi a})$, and the normalized EDIF $K_{IV}/(D^\infty\sqrt{\pi a})$ evaluated at the right crack tip, using methods I–III without extra correction terms (M-I (NC), M-II (NC), M-III (NC)) and with extra correction terms (M-I (WC), M-II (WC), M-III (WC)) with respect to various integral domain sizes. It can be observed that the contribution of extra correction terms is more significant for larger integral domains. This is due to the reason that, as the integral domain size shrinks to the crack tip contribution of extra correction terms becomes less as in the limit $r \to 0$, extra correction terms $\to 0$, which is proved in earlier section.

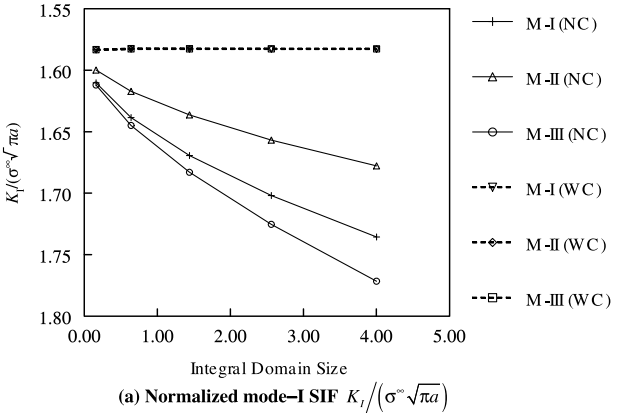

(a) Normalized mode–I SIF $K_I/\left(\sigma^\infty\sqrt{\pi a}\right)$

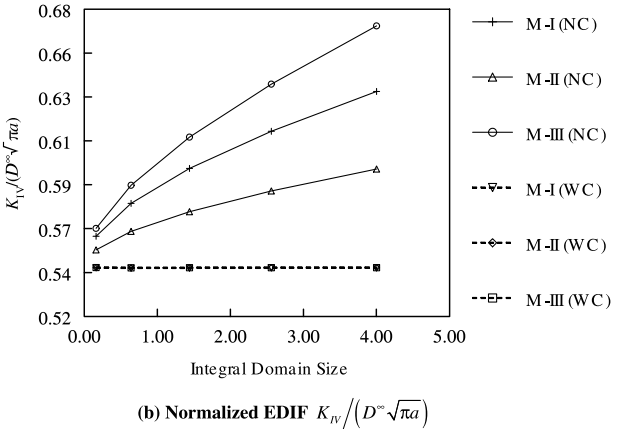

(b) Normalized EDIF $K_{IV}/\left(D^\infty\sqrt{\pi a}\right)$

Fig. 9. Significance of extra correction terms under type 1 loading combination (example 1).

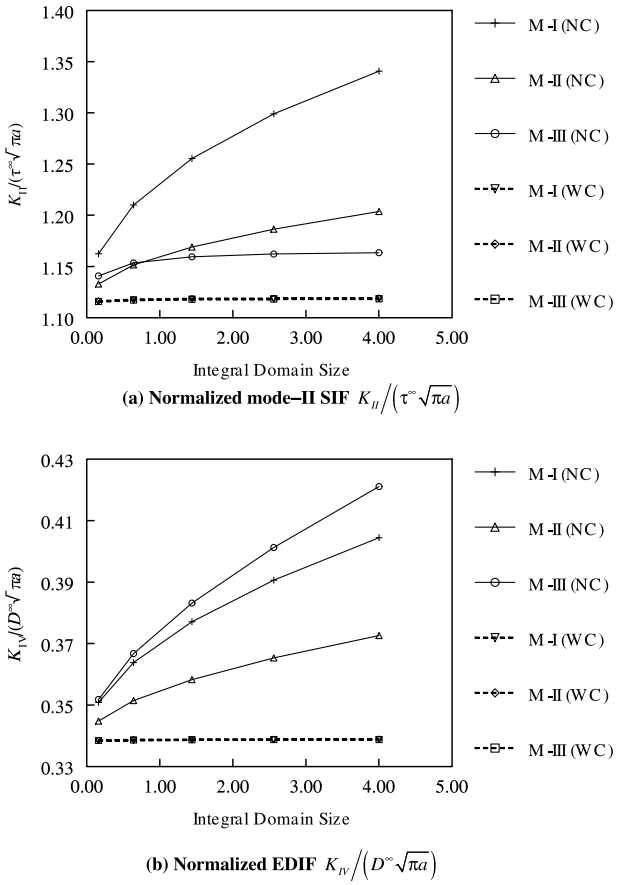

Fig. 10. Significance of extra correction terms under under type 2 loading combination (example 1).

5.2. Example 2: finite inclined crack in an infinite medium

The geometric configuration with crack inclination angle $\alpha = 0.25\pi$ and the loads considered in this study are shown in Fig. 11(a). Loading combination of the far-field normal load σ^{∞} and the far-field electrical displacement load D^{∞} is studied. The poling direction is assumed to be in x_2 direction. Fig. 11(b) shows the FE model discretization involving 2416 nodes, 736 eight-noded quadrilateral elements, and 64 focused quarter-point six-noded triangular elements adopted for the evaluation of intensity factors using the interaction integrals based on the proposed three formulations (in Eqs. (46), (50) and (54)). The SIFs and EDIF are also computed using DEM with $L_e = 0.02a$, using FE model discretization involving a total of 2808 nodes over the entire domain.

Tables 5–7, show respectively the normalized mode-I SIF $K_{\mathrm{I}}/(\sigma^{\infty}\sqrt{\pi a})$, the normalized mode-II SIF $K_{\mathrm{II}}/(\sigma^{\infty}\sqrt{\pi a})$, and the normalized EDIF $K_{\mathrm{IV}}/(D^{\infty}\sqrt{\pi a})$ evaluated at the right crack tip, using the proposed methods I–III and DEM for various combinations of the loading combination parameter λ and the non-homogeneity parameter η. A domain size of 1.6 units $\times$ 1.6 units is taken around the right crack tip to compute the $\widetilde{M}^{(1,2)}$-integral. It can be observed that irrespective of the values of λ and ηa, all the three methods predicted almost the same value of the normalized intensity factors which matches well with those obtained using DEM.

6. Summary and conclusions

The paper presents domain forms of the interaction integrals based on three independent formulations for computation of the SIFs and EDIF for cracks in the FGPMs. Conservation integrals of J-type are derived based on the governing equations for piezoelectric media and the crack tip asymptotic fields of homogeneous piezoelectric medium as auxiliary fields. Each of the formulations differs in the way auxiliary fields are imposed in the evaluation of the interaction integral and each of them results in a consistent form of the interaction integral in the sense that extra terms naturally appear in their derivation to compensate for the difference in the chosen crack tip asymptotic fields of homogeneous and functionally graded piezoelectric medium. The additional terms play an important role of ensuring domain independence of the presented interaction integrals. Accuracy of the predicted intensity factors using the interaction integrals based on three formulations is investi-

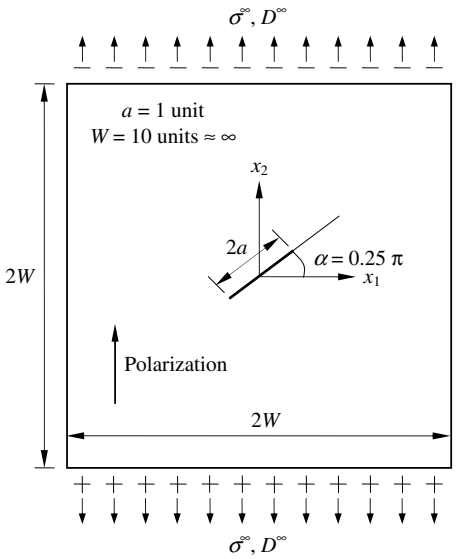

(a) Geometry and loads for inclined crack in an infinite medium under far-field normal load σ^{∞} and far-field electrical displacement load D^{∞}

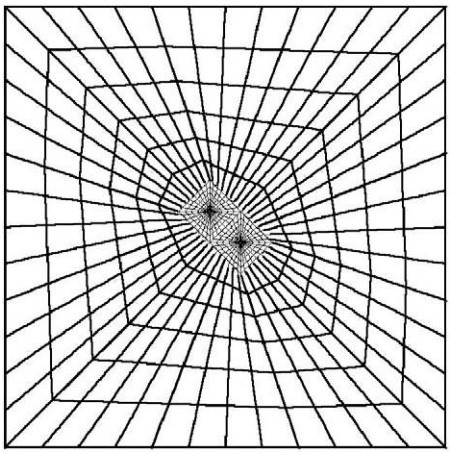

(b) FEM discretization (2416 nodes, 736 8-noded quadrilateral elements, and 64 focused quarter-point 6-noded triangular elements)

Fig. 11. Finite inclined crack in an infinite medium (example 2).

gated by comparing with those obtained by using displacement extrapolation method by means of two examples. Very stable results of intensity factors are obtained regardless of the type of the auxiliary field. The interaction integrals based on all three independent formulations predicted almost the same value of the normalized intensity factors irrespective of the values of the loading combination parameter and the non-homogeneity parameter. However, the interaction integral based on

Table 5
Normalized mode-I stress intensity factor $K_I/(\sigma^{\infty}\sqrt{\pi a})$ under far-field normal load σ^{∞} and far-field electrical displacement load D^{∞} (example 2)

ηa	$\lambda = -5$				$\lambda = 0$				$\lambda = 5$			
	Method-I	Method-II	Method-III	DEM	Method-I	Method-II	Method-III	DEM	Method-I	Method-II	Method-III	DEM
−0.5	0.841996	0.841994	0.841993	0.843780	0.850252	0.850255	0.850253	0.852030	0.841996	0.841994	0.841993	0.860281
−0.25	0.829786	0.829793	0.829792	0.831565	0.770122	0.770132	0.770131	0.771724	0.710457	0.710471	0.710469	0.711882
−0.125	0.624815	0.624820	0.624819	0.626190	0.596311	0.596318	0.596317	0.597555	0.567807	0.567816	0.567815	0.568919
0	0.506144	0.506144	0.506144	0.507273	0.506087	0.506087	0.506087	0.507139	0.506031	0.506031	0.506031	0.507004
0.125	0.721933	0.721925	0.721925	0.723461	0.666742	0.666733	0.666733	0.668097	0.611551	0.611540	0.611541	0.612733
0.25	1.093619	1.093597	1.093597	1.095835	0.972689	0.972667	0.972667	0.974626	0.851760	0.851737	0.851736	0.853416
0.5	1.374289	1.374242	1.374248	1.376936	1.320130	1.320082	1.320088	1.322656	1.265971	1.265921	1.265927	1.268375

Table 6
Normalized mode-II stress intensity factor $K_{II}/(\sigma^{\infty}\sqrt{\pi a})$ under far-field normal load σ^{∞} and far-field electrical displacement load D^{∞} (example 2)

ηa	$\lambda = -5$				$\lambda = 0$				$\lambda = 5$			
	Method-I	Method-II	Method-III	DEM	Method-I	Method-II	Method-III	DEM	Method-I	Method-II	Method-III	DEM
−0.5	−0.276975	−0.276553	−0.276606	−0.273079	−0.304114	−0.303679	−0.303737	−0.299949	−0.331253	−0.330805	−0.330869	−0.326818
−0.25	−0.485569	−0.485332	−0.485384	−0.479746	−0.480176	−0.479949	−0.480001	−0.474510	−0.474784	−0.474567	−0.474618	−0.469275
−0.125	−0.513980	−0.513881	−0.513909	−0.508107	−0.505991	−0.505893	−0.505922	−0.500283	−0.498002	−0.497906	−0.497934	−0.492460
0	−0.504262	−0.504262	−0.504262	−0.498630	−0.504306	−0.504306	−0.504306	−0.498735	−0.504351	−0.504351	−0.504351	−0.498840
0.125	−0.496485	−0.496600	−0.496571	−0.490881	−0.498528	−0.498638	−0.498607	−0.492978	−0.500570	−0.500675	−0.500644	−0.495074
0.25	−0.444048	−0.444366	−0.444306	−0.438944	−0.453071	−0.453361	−0.453301	−0.447947	−0.462094	−0.462357	−0.462296	−0.456950
0.5	−0.138923	−0.139609	−0.139546	−0.137318	−0.176334	−0.177003	−0.176931	−0.174343	−0.213745	−0.214397	−0.214316	−0.211367

Table 7
Normalized electric displacement intensity factor $K_{IV}/(D^{\infty}\sqrt{\pi a})$ under far-field normal load σ^{∞} and far-field electrical displacement load D^{∞} (example 2)

ηa	$\lambda = -5$				$\lambda = 5$			
	Method-I	Method-II	Method-III	DEM	Method-I	Method-II	Method-III	DEM
−0.5	0.036435	0.036446	0.036460	0.035892	0.285948	0.285908	0.285923	0.285193
−0.25	0.266658	0.266644	0.266659	0.265409	0.511087	0.511056	0.511078	0.509162
−0.125	0.525881	0.525863	0.525874	0.523803	0.632715	0.632695	0.632710	0.630136
0	0.707182	0.707182	0.707182	0.704455	0.710371	0.710371	0.710371	0.707400
0.125	0.624432	0.624457	0.624442	0.621784	0.701463	0.701489	0.701471	0.698630
0.25	0.397042	0.397073	0.397051	0.394830	0.619102	0.619151	0.619123	0.616902
0.5	0.156959	0.156979	0.156943	0.154952	0.375867	0.375942	0.375922	0.375477

constant constitutive tensor formulation requires the derivatives of the actual stress and electrical displacement fields, which in turn requires second order derivatives of finite element shape functions. This requirement needs additional effort and also may introduce accuracy problems with C^0 elements. As, in the present study eight-noded quadrilateral elements and six-noded triangular elements are adopted, all the three methods resulted in almost the same value of the normalized intensity factors to the significant digit accuracy considered.

Acknowledgement

The first author would like to acknowledge the fellowship of the Alexander von Humboldt Foundation during course of this research.

References

Anderson, T.L., 2005. Fracture Mechanics: Fundamentals and Applications. CRC Press, Inc.
Chen, J., Liu, Z.X., Zou, Z.Z., 2003. Electromechanical impact of a crack in a functionally graded piezoelectric medium. Theoretical and Applied Fracture Mechanics 39, 47–60.
Cherepanov, G.P., 1977. Invariant *G*-integrals and some of their applications in mechanics. Journal of Applied Mathematics and Mechanics 41, 397–410.
Dolbow, J., Gosz, M., 2002. On the computation of mixed-mode stress intensity factors in functionally graded materials. International Journal of Solids and Structures 39, 2557–2574.
Eischen, J.W., 1987. Fracture of nonhomogeneous materials. International Journal of Fracture 34, 3–22.
Enderlein, M., Ricoeur, A., Kuna, M., 2005. Finite element techniques for dynamic crack analysis in piezoelectrics. International Journal of Fracture 134, 191–208.
Jin, Z.H., Noda, N., 1994. Crack tip singular fields in nonhomogeneous materials. Transactions of the ASME, Journal of Applied Mechanics 61, 738–740.
Kim, J.H., Paulino, G.H., 2003. The interaction integral for fracture of orthotropic functionally graded materials: evaluation of stress intensity factors. International Journal of Solids and Structures 40, 3967–4001.
Kuna, M., 2006. Finite element analyses of cracks in piezoelectric structures: a survey. Archive of Applied Mechanics 76, 725–745.
Li, C., Weng, G.J., 2002. Antiplane crack problem in functionally graded piezoelectric materials. Transactions of the ASME, Journal of Applied Mechanics 69, 481–488.
Ma, L., Wu, L.Z., Zhou, Z.G., Guo, L.C., 2005. Fracture analysis of a functionally graded piezoelectric strip. Composite Structures 69, 294–300.
Pak, Y.E., 1990. Crack extension force in a piezoelectric material. Transactions of the ASME, Journal of Applied Mechanics 57, 647–653.
Pak, Y.E., 1992. Linear electro-elastic fracture mechanics of piezoelectric materials. International Journal of Fracture 54, 79–100.
Pak, Y.E., Herrmann, G., 1986. Conservation laws and the material momentum tensor for the elastic dielectric. International Journal of Engineering Science 24, 1365–1374.
Park, S.B., Sun, C.T., 1995. Effect of electric field on fracture of piezoelectric ceramics. International Journal of Fracture 70, 203–216.
Paulino, G.H., Kim, J.H., 2004. A new approach to compute T-stress in functionally graded materials by means of the interaction integral method. Engineering Fracture Mechanics 71, 1907–1950.
Rao, B.N., Rahman, S., 2003a. Meshfree analysis of cracks in isotropic functionally graded materials. Engineering Fracture Mechanics 70, 1–27.
Rao, B.N., Rahman, S., 2003b. An interaction integral method for analysis of cracks in orthotropic functionally graded materials. Computational Mechanics 32, 40–51.
Ricoeur, A., Kuna, M., 2003. Influence of electric fields on the fracture of ferroelectric ceramics. Journal of the European Ceramic Society 23, 1313–1328.
Sladek, J., Sladek, V., Zhang, C., Solek, P., Pan, E., 2007. Evaluation of fracture parameters in continuously nonhomogeneous piezoelectric solids. International Journal of Fracture 145, 313–326.

Sosa, H., 1991. Plane problems in piezoelectric media with defects. International Journal of Solids and Structures 28, 491–505.
Ueda, S., 2006. A finite crack in a semi-infinite strip of a grade piezoelectric material under electric loading. European Journal of Mechanics A/Solids 25, 250–259.
Ueda, S., 2007. Electromechanical impact of an impermeable parallel crack in a functionally graded piezoelectric strip. European Journal of Mechanics A/Solids 26, 123–136.
Ueda, S., 2008. Functionally graded piezoelectric strip with a penny-shaped crack under electromechanical loadings. European Journal of Mechanics A/Solids 27, 50–60.
Wang, B.L., Noda, N., 2001. Thermally induced fracture of a smart functionally graded composite structure. Theoretical and Applied Fracture Mechanics 35, 93–109.
Wang, B.L., Zhang, X.H., 2004. A mode III crack in functionally graded piezoelectric material strip. Transactions of the ASME, Journal of Applied Mechanics 71, 327–333.
Wu, C.M., Kahn, M., Moy, W., 1996. Piezoelectric ceramics with functionally gradients: a new application in material design. Journal of American Ceramics Society 79, 809–812.
Zhu, X., Xu, J., Meng, Z., Zhu, J., Zhou, S., Li, Q., Liu, Z., Ming, N., 2000. Microdisplacement characteristics and microstructures of functionally gradient piezoelectric ceramic actuator. Materials and Design 21, 561–566.